

**ROCK PHYSICS MODELING OF AN UNCONSOLIDATED
SAND RESERVOIR**

A Thesis
Presented to
the Faculty of the Department of Earth
and Atmospheric Sciences
University of Houston

In Partial Fulfillment
of the Requirements for the Degree
Master of Science

By
Jadranka Milovac
December 2009

**ROCK PHYSICS MODELING OF AN UNCONSOLIDATED
SAND RESERVOIR**

Jadranka Milovac

APPROVED:

Dr. John P. Castagna, Chairman

Dr. De-hua Han

Dr. Evgeny Chesnokov

Dr. Tad Smith

Dean, College of Natural Sciences and Mathematics

ACKNOWLEDGEMENTS

I would like to take this opportunity to thank all my committee members, and express my deepest gratitude to my advisors, Dr. John Castagna and Dr. De hua-Han for their guidance, encouragement, and enthusiasm through all these years.

I want to thank Marathon Oil Company, Worldwide Petrophysics group, and my supervisor Jeff Hamman for being patient and supporting me in my efforts to finish my thesis work.

I wish to thank my friends from University of Houston for their advices and support, as well.

Finally, I want to thank my parents, brother, and my fiancé for believing in me and being always by my side.

**ROCK PHYSICS MODELING OF AN UNCONSOLIDATED
SAND RESERVOIR**

An Abstract of a Thesis
Presented to
the Faculty of the Department of Earth
and Atmospheric Sciences
University of Houston

In Partial Fulfillment
of the Requirements for the Degree
Master of Science

By
Jadranka Milovac
December 2009

ABSTRACT

A rock physics model has been built for an unconsolidated Gulf of Mexico reservoir, respecting the assumption that if well log data points fall close to a theoretical line in velocity-porosity or modulus-porosity planes, then the internal structure of a rock is similar to the idealized structure predicted by theoretical model. We hypothesize that the rock physics parameters for certain areas are predictable and smoothly varying, so that it is possible to determine them by using well log measurements and rock physics theory.

Several models are compared. Krief and Critical porosity models predict too stiff elastic parameters and can not be used for predicting elastic properties of unconsolidated formations. Hertz-Mindlin theory estimates bulk modulus accurately but overpredicts shear modulus, which was adjusted applying slip-factor correction, and as such it was used as a final model for Hoover sands. From the log data at Hoover field, the equation is derived for dry frame properties as a function of porosity and shaliness. The equation shows good fit with Murphy data (Murphy, 1993) in high porosity range.

Hertz-Mindlin theory, combined with modified Hashin-Shtrikman lower bound and Gassmann fluid substitution, is applied to create a rock physics framework for quantitative seismic analysis, where elastic properties are expressed in terms of pressure, porosity and saturation. The framework gives a rough estimate on porosity and less reliable estimate on saturation.

CONTENT

1. INTRODUCTION	1
1.1 RESEARCH OBJECTIVE	1
1.2 BACKGROUND AND MOTIVATION	1
1.3 THESIS OVERVIEW	4
2. ROCK PHYSICS MODELING OF UNCONSOLIDATED SANDS	5
2.1 THEORETICAL MODELS OVERVIEW	6
2.1.1 Hertz-Mindlin theory	8
2.1.2 Hashin-Strikman bounds.....	11
2.1.3 Gassmann fluid substitution.....	13
2.1.4 Model results	17
2.2 HEURISTIC MODELS	26
2.2.1 Critical porosity model.....	26
2.2.2 Krief model	28
2.2.3 Model results	28
3. ELASTIC PROPERTIES: HOOVER FIELD, GULF OF MEXICO	35
3.1 DATA SET OVERVIEW: HOOVER FIELD, GULF OF MEXICO.....	35
3.2 ELASTIC PROPERTIES AT HOOVER FIELD (WELL LOG DATA).....	38
3.2.1 Petrophysical analysis	45
3.2.2 Definition of rock composite (Sand-Shale system).....	47
3.2.3 Inverting for rock frame properties using Gassmann fluid substitution	48
3.3 RESULTS AND DISCUSSION.....	51
3.4 ROCK FRAME MODELS COMPARISON.....	56
4. CROSS-PLOT ANALYSIS: ROCK PHYSICS TEMPLATES	58
4.1 METHODOLOGY AND ALGORITHM.....	60
4.2 FINAL PLOT AND APPLICATION	62
4.3 PROBABILISTIC MODELING	64
5. CONCLUSION	69
REFERENCES	71
APPENDIX I: COORDINATION NUMBER	75
APPENDIX II: EFFECTIVE PRESSURE ESTIMATION	76
APPENDIX III: INDONESIA EQUATION	77

TABLE OF FIGURES

Figure 1. Physical meaning of critical porosity (Nur <i>et al.</i> , 1998).	1
Figure 2. Dry frame elastic moduli and dry velocities with respective models showing deflection points at the consolidation porosity of 30% (Vernik, 1998).	3
Figure 3. End-member bulk moduli: a) High porosity end-member; b) Hashin-Shtrikman lower bound interpolation (Avseth <i>et al.</i> , 2006).	9
Figure 4. Estimated bulk modulus and density of oil and brine (FLAG program).	14
Figure 5. Theoretically predicted “dry” bulk and shear moduli as a function of porosity for sandstones with porosity ranging from 0.20 to 0.36 ($P_{\text{eff}} = 22$ MPa).	18
Figure 6. Theoretically predicted “dry” bulk vs. shear modulus. Red curve indicates the direction of porosity decrease.	19
Figure 7. Theoretically predicted “dry” P-wave and S-wave velocities as a function of porosity for sandstones with porosity ranging from 0.20 to 0.36 ($P_{\text{eff}} = 22$ MPa).	19
Figure 8. Theoretically predicted bulk modulus for different water saturation. Logged data trend lines superimposed for the porosity 30.5-33.5% (light green and light blue trend lines for oil and wet sand, respectively).	20
Figure 9. Theoretically predicted P- and S-wave velocities as a function of porosity for wet, oil and dry case ($P_{\text{eff}} = 22$ MPa). Superimposed: logged data for the porosity 30.5-33.5%	21
Figure 10. Theoretically predicted V_p/V_s vs. V_p velocities ($P_{\text{eff}} = 22$ MPa).	22
Figure 11. Moduli after slip-factor correction (shear modulus reduced).	23
Figure 12. Slip-corrected moduli superimposed with Ottawa and Troll sands (Blangy, 1992) in modulus vs. porosity plane.	23
Figure 13. Theoretically predicted P- and S-wave velocities after slip-factor correction, superimposed with logged data for the range 30.5-33.5% porosity.	24
Figure 14. Theoretically predicted V_p/V_s ratio after slip-factor correction.	25
Figure 15. Dry bulk modulus vs. porosity: Krief and Critical porosity model.	29
Figure 16. Bulk modulus vs. porosity: Krief, Critical porosity model and logged data comparison: DRY (left), OIL saturated (middle), WATER saturated (right). Porosity range 31-33%.	30
Figure 17. “Dry” P-wave and S-wave velocities vs. porosity: Krief and Critical porosity models.	31

Figure 18. Dry velocity vs. porosity: Krief and Critical porosity model. P-wave (left) and S-wave (right). Porosity range 30-35%.....	32
Figure 19: P-wave velocity vs. porosity: Krief, Critical porosity model and logged data comparison: dry, oil saturated, and water saturated. Porosity range 31-33%.....	33
Figure 20: S-wave velocity vs. porosity: Krief, Critical porosity model and logged data comparison: dry, oil saturated, and water saturated. Porosity range 31-33%.....	34
Figure 21. The Diana mini-basin. A) Location: western Gulf of Mexico 255 km south of Galveston. B) Five discoveries: Diana, South Diana, Marshall, Madison and Hoover. C) Combined structure and amplitude extraction for the upper Pliocene A-50 reservoir (Sullivan <i>et al.</i> , 2004).....	36
Figure 22. Seismic section at well locations (vertical scale is time, in ms). Seven wells penetrate Hoover oil reservoir, four of which are presented.	37
Figure 23. The composite log: Hoover-1, whole interval logged, 9100-12950 ft (2774-3947 m) MD.	38
Figure 24. <i>In situ</i> moduli vs. porosity: bulk modulus (left) and shear modulus (right).	40
Figure 25. <i>In situ</i> velocities vs. porosity: P-wave velocity (left) and S-wave velocity (right). Right figure is color-coded by saturation.	40
Figure 26. Comparing P-wave velocities (left) and densities (right) of shales (colored green) and wet sands (colored red).	41
Figure 27. V_p vs. V_s (as logged) with different trend line superimposed. a) Left figure: mudrock line, Castagna-shales, Castagna-sands. b) Right figure: Williams-shale, Williams-sands, regression on <i>in situ</i> data for sands, shales and sands-and-shales.	42
Figure 28. V_p/V_s ratio vs. DTC cross-plot: a) shales, b) wet sands, c) reservoir sands: oil and water (cross-plot idea from Brie <i>et al.</i> , 1995).	43
Figure 29. Composite log and petrophysical analysis result for Hoover-1, reservoir zone: 12792-12895 ft (3899-3930 m).....	45
Figure 30. The Neutron-Density cross-plot for interval 12650-12900 ft (3856-3932 m).....	46
Figure 31. The sand-shale composite (Truman, 1989).	47
Figure 32. The sand-shale system, as modeled.	49
Figure 33. Mixing moduli using Hill average (color-coded by volume of shale).	50
Figure 34. Estimated “dry” bulk modulus, K_{DRY} , presented as green curve in track five. K_{SAT} is bulk modulus at initial saturation (black curve in track five), and Hill average for mineral bulk modulus, K_{MINH} (red curve in track five).....	52
Figure 35. “Dry” bulk modulus determined from logs superimposed with Hashin-Shtrikman upper and lower bounds for rocks saturated with different fluids: water, oil, and gas, at surface condition.....	53

Figure 36. Comparison between derived regression equation and Murphy curve for clean sands, in bulk modulus vs. porosity plane.....	54
Figure 37. Log-derived dry bulk modulus superimposed with theoretically predicted curve.	56
Figure 38. “Dry” modulus vs. porosity plane. Comparison between Kdrys for: Kdry derived from Hoover logged data with effective porosity (KDRYE), effective porosity KDRYE constrained with Kdry-to- μ dry ratio (KB_dry_PSEUDO; Smith et al. 2003), Kdry from Krief (Kdry_KRIEF), CPM (Kdry_Critical), Kdry derived from logged data with total porosity (KB_dry).	57
Figure 39. Rock physics template in Vp/Vs vs. AI (Odegaard <i>et al.</i> , 2004).	58
Figure 40. Rock physics template algorithm.	61
Figure 41. Rock physics template in Vp/Vs vs. AI domain for Hoover reservoir (oil sand, wet sand below oil-water contact, shales around the reservoir. Depth 12780-12900 ft (3923-3932 m).	62
Figure 42. Rock physics template in Vp/Vs vs. AI for Hoover reservoir (oil sand, wet sand below oil-water contact, shales around the reservoir. Depth 12780-12900 ft (3923-3932 m).	63
Figure 43. Input parameters distribution	65
Figure 44. Rock frame properties. X-axis: porosity, y-axis: dry rock properties (P-wave and S-wave velocities, Vp-Vs ratio, Bulk modulus, Shear modulus, Bulk-Shear modulus ratio).	66
Figure 45. Rock properties for range of saturations, from Soil=1 to Sw=1. X-axis: porosity, y-axis: dry rock properties (P-wave and S-wave velocities, Vp-Vs ratio, Bulk modulus, Shear modulus, Bulk-Shear modulus ratio).	67
Figure 46. Final plot Vp-Vs vs AI cross-plot. Color coded by water saturation: red=100% brine; blue=100% oil.	68
Figure 47. Geometric properties of sphere pack: coordination number vs. porosity.....	75
Figure 48. Pressure gradient analysis for Hoover-1 (MDT data).	76

1. INTRODUCTION

1.1 Research objective

This thesis represents a rock physics study of an unconsolidated sand reservoir. The main goal is to build a site-specific rock physics model using appropriate theories to explain the observed velocity trends in unconsolidated formations. Several models are compared and discussed, and the final model is incorporated into an algorithm for creating a framework for quantitative seismic interpretation. This is applied to the Hoover field, in the deepwater Gulf of Mexico.

1.2 Background and motivation

For most clastic rocks, there is a porosity that separates their mechanical and acoustic behavior into two domains (Figure 1). Some authors refer to it as critical porosity, Φ_c (e.g., Nur *et al.*, 1998). For the porosities lower than Φ_c mineral grains are load bearing, while for the porosities greater than Φ_c the fluid phase is assumed to support the load and the mineral grains are in suspension (Nur, 1992).

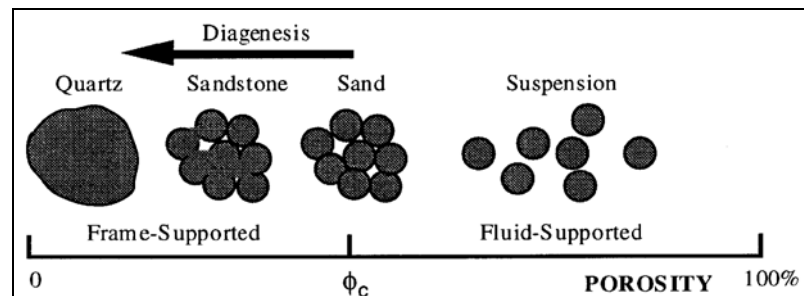


Figure 1. Physical meaning of critical porosity (Nur *et al.*, 1998).

In fact, numerous studies have shown that sediments above the critical porosity often exhibit some rigidity, and therefore cannot be strictly treated as suspension (Raymer *et al.*, 1980).

In a geologic context, Φ_c describes the sediment when it is first deposited and is related to grain sorting and angularity. Later, compaction and diagenesis reduce the porosity and increase the elastic stiffness.

From the perspective of elastic properties, consolidated and unconsolidated formations have different trend behavior (Figure 2). Values of elastic moduli in consolidated sandstones are in approximately linear relation to the porosity (Nur *et al.*, 1991). Several authors have established important relationships between elastic properties and reservoir parameters, such as porosity and clay content (*e.g.*, Han, 1986; Marion, 1992), diagenesis (*e.g.*, Jizba, 1991; Dvorkin and Nur, 1996), fractures (*e.g.*, Chen, 1995; *etc.*), lithology (*e.g.*, Castagna *et al.*, 1985; Blangy, 1992; Greenberg and Castagna, 1992), as well as pore fluids (*e.g.*, Wang and Nur, 1990; Batzle and Wang, 1992).

On the other hand, even in the range of high porosity clastic rocks, there is a distinction between high porosity rocks depending on the distribution of intergranular material. Thus the texture becomes a very important parameter. A small amount of cement on a grain contact will significantly stiffen the frame of the rock and greatly increase velocity (Dvorkin *et al.*, 1996). One of the consequences is that seismic signatures of unconsolidated sands filled with water can be very similar to those of high-

porosity cemented rocks saturated with hydrocarbons. This provides an impetus to try to develop a site-specific model for unconsolidated formations which might be useful in distinguishing the two.

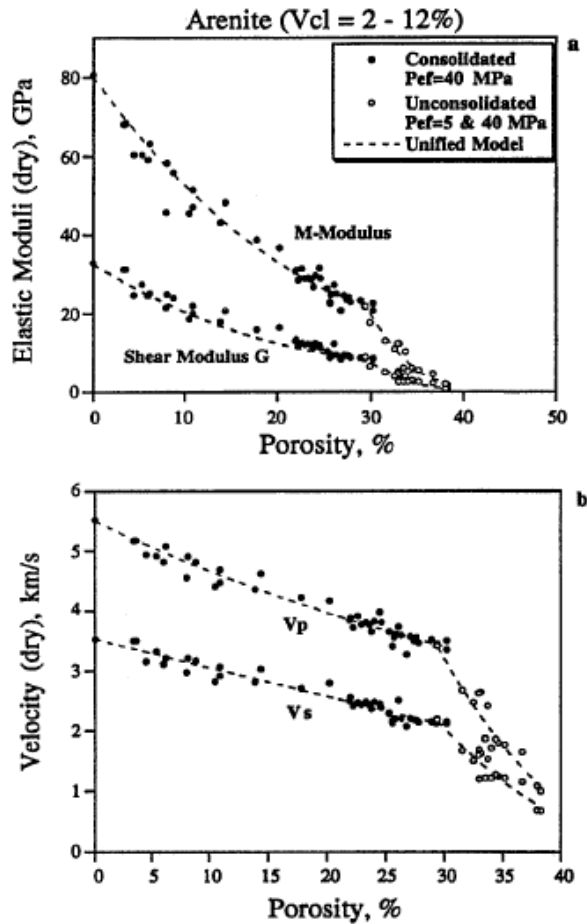


Figure 2. Dry frame elastic moduli and dry velocities with respective models showing deflection points at the consolidation porosity of 30% (Vernik, 1998).

As velocities in unconsolidated rocks are highly dependent upon saturation and pressure, an accurate and well calibrated model might be used for time-lapse seismic monitoring, reflecting the changes within the reservoir during production (if the changes are large enough).

1.3 Thesis overview

The first part of this thesis (Section 2) consists of developing a rock physics model: effective medium models are used to predict velocities in unconsolidated sands, and compared with the heuristic, Krief and Critical porosity models (non-linear and linear porosity-dry bulk modulus relationship, respectively). An overview of some potential pitfalls of the methods is given.

The second part (Section 3) covers estimation of elastic rock frame properties from real data, the Hoover field, Gulf of Mexico. Gassmann's equation is used to determine rock frame properties in shaly-sand formations, defining a site-specific sand-shale system, and extracting shale properties from log data.

The last part (Section 4), illustrates the possible applications of the developed methodology: the benefits of rock physics models in interpretation of seismic inversion results. It, also, provides the procedure for creating a rock physics template through deterministic and probabilistic approaches.

2. ROCK PHYSICS MODELING OF UNCONSOLIDATED SANDS

In general, elastic properties of rocks are controlled by lithology (composition and texture), porosity (amount and type), pore fluids, depth (differential pressure, temperature, age and lithification), frequency, anisotropy, *etc.* (Table 1). All the parameters do not have the same importance, and the main controlling parameters can be, and usually are, different in different geologic environments.

To estimate the velocities in granular materials, we must account for porosity, pressure, friction, and coordination number. The effective bulk and shear moduli are computed using a combination of effective medium theory for modeling the rock frame (“dry” condition), and Gassmann fluid substitution for building a fluid fill model for particular fluid type (“saturated” condition).

Table 1. Controlling factors of seismic properties in sedimentary rocks (Wang, 2001).

Rock properties	Fluid properties	Environment
Compaction	Viscosity	Frequency
Consolidation	Density	Stress history
Age	Wettability	Depositional environment
Cementation	Fluid composition	Temperature
Texture	Phase	Reservoir process
Bulk density	Fluid type	Production history
Clay content	Gas-oil, gas-water ratio	Layer geometry
Anisotropy	Saturation	Differential pressure
Fractures		
Porosity		
Lithology		
Pore shape		

2.1 Theoretical models overview

To predict effective elastic moduli of a mixture of grains and pores, we generally need to specify (Mavko *et al.*, 1998) volume fractions of the constituents, grain and pore arrangements, and elastic moduli of the constituents. All theoretical models can be roughly classified into several categories (Avseth *et al.*, 2005):

- Inclusion models: which approximate the rock as an elastic solid with cavities, where cavities represent pore space. For the vast majority of models pore cavities are ellipsoidal (Kuster and Toksoz, 1974; O’Connell and Budiansky, 1974; *etc.*). Berryman (1980) expanded this approach into considering both pores and grains as ellipsoidal “inclusions”. There are some other theories which address inclusion cavities as non-ellipsoidal in shape (Mavko, 1980); or as infinite planes (Schoenberg, 1983).
- Contact models: which approximate the rock as a collection of separate grains, whose elastic properties are determined by deformability and stiffness of their grain-to-grain contact. They are based on Hertz-Mindlin model (Mindlin, 1949): Walton, 1987; Digby, 1981; *etc.*). Dvorkin and Nur (1996) added mineral cement at contact grains into the models.
- Computational models: in which grain-pore microgeometry is determined by thin-section and CT-scan image.
- Bounds: are robust and free of approximations, other than to treat the rock as an elastic composite. They are valuable mixing laws. Most often used are Voigt-Reuss and Hashin-Shtrikman bounds.

- Transformations: are free of geometric assumptions. Two of the most widely used are Gassmann's fluid substitution (Gassmann, 1951), and the Berryman and Milton (1991) - composite of two porous media having separate mineral and dry-frame moduli.

In order to predict velocity of a rock with known porosity, mineralogical composition and elastic moduli of mineral constituents, and having no information about grain and pore arrangements, the most appropriate way is to use upper and lower bounds of elastic moduli (Mavko *et al.*, 2003). Well logs provide data about constituents of formation and their volume fraction, while they provide relatively little information about grains and pore structures. Also, there is a minimum amount of *a priori* information that is required as a geological constrain on modeling:

- Lithology: a siliciclastic environment in the particular case at the Hoover field, represented by clean sands, shaly sands and shales;
- Pressure regime: the water depth and burial depth determine confining, pore, and effective pressure;
- Area/basin characteristics: which are related to shale-trend selection (gamma-ray reading) in a particular basin.

For this thesis work, a theoretical model is used to predict the high porosity end-members, a modified Hashin-Shtrikman lower bound for extrapolation between zero-porosity and high porosity end-members (heuristic model), and Gassmann's equation for calculating elastic moduli at different saturation conditions (theoretical model). Modeled

results are compared with an empirical model (Blangy, 1993) and with the elastic properties estimated from the Hoover field (Section 3).

2.1.1 Hertz-Mindlin theory

The elastic modulus at high porosity (usually critical porosity) is modeled as an elastic sphere pack influenced by net confining pressure using *Hertz-Mindlin theory* (Dvorkin *et al.*, 1996). It has been shown that this theory gives accurate pressure dependence for any unconsolidated sediment when the porosity reduction is caused by mechanical compaction (Avseth *et al.*, 2001), and it is given by:

$$K_{HM} = \left[\frac{n^2(1-\Phi_c)^2 \mu^2}{18\pi^2(1-\nu)^2} P \right]^{\frac{1}{3}} \quad (1)$$

$$\mu_{HM} = \frac{5-4\nu}{5(2-\nu)} \left[\frac{3n^2(1-\Phi_c)^2 \mu^2}{2\pi^2(1-\nu)^2} P \right]^{\frac{1}{3}}, \quad (2)$$

where,

K_{HM} , μ_{HM} = dry rock bulk and shear moduli, respectively, at initial porosity Φ_c ;

n = coordination number;

P = net confining pressure, which is equal to effective pressure (assumes Biot coefficient is equal to one);

μ = shear modulus for solid phase (mineral modulus);

ν = Poisson's ratio for solid phase.

The coordination number (n) of the granular assembly is defined as the average number of contacts per grain (Mavko *et al.*, 1998). Coordination number increases with decreasing porosity, which is the result of more efficient packing under increasing confining pressure. The dependence of n on porosity and pressure is not explicitly accounted for in the theory. Murphy (1982) proposed an empirical n -porosity relation based on laboratory observations from various sources (Appendix I). For this thesis work, as we are modeling a single end-member only, a constant relationship between porosity and contacts per grain has been used (dense random packing of grains was assumed).

The grain contact model assumes identical homogeneous, isotropic, elastic spherical grains, and strains that are small (Mavko *et al.*, 1998).

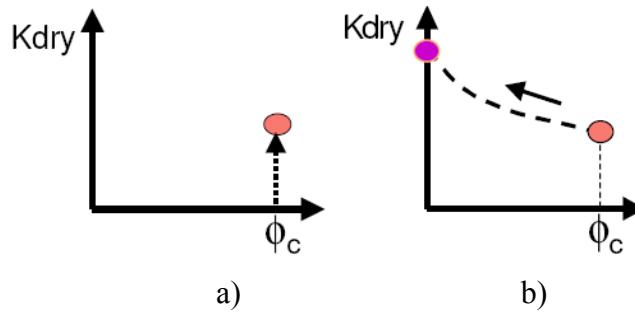


Figure 3. End-member bulk moduli: a) High porosity end-member; b) Hashin-Shtrikman lower bound interpolation (Avseth *et al.*, 2006).

High porosity end-members (bulk and shear moduli) do not necessarily have to be calculated from the Hertz-Mindlin theory. They can be measured experimentally on high porosity sands from the given reservoir, or estimated from well log data. It has been shown that theoretical data for shear modulus are too large and it should be adjusted using a slip factor (Deng *et al.*, 2006). The initial assumption according to Hertz-Mindlin

theory is no-slip effect at the contact surface between two grains. The spherical grains are first pressed together; a tangential force is applied afterwards. The no-slip assumption results in the shear-wave velocity being overpredicted, and the V_p/V_s ratio being underpredicted, compared with the observed laboratory and well log measurements. Bachrach *et al.* (2000) proposed 50% grains with zero tangential stiffness. However, it is difficult to determine what fraction of grains has zero tangential stiffness. It also predicts a lower pressure exponent for velocities ($V \sim p^{1/6}$) than is generally observed in data. A common approach to improve the model is to adjust the contact friction and coordination number, treating both as free parameters.

The applicability of Hertz-Mindlin theory on shales can be debated. It violates the assumption of the spherical grains in contact, as shales contain mainly clay particles which are platy. However, when calculating the effective bulk and shear moduli of a dry sphere pack, coordination number takes into account the shape of the grain, and it has been found that this theory works fairly well for shales as well as for sands (Avseth *et al.*, 2005). Shales with high porosity have relatively small coordination number, and vice versa.

2.1.2 Hashin-Strikman bounds

The *Hashin-Shtrikman bounds* provide the narrowest range of elastic moduli without specifying geometries of constituents. Hashin-Shtrikman bounds are given by (Mavko *et al.*, 1998):

$$K_{HS\pm} = K_1 + \frac{f_2}{(K_2 - K_1)^{-1} + f_1 \left(K_1 + \frac{4}{3} \mu_1 \right)^{-1}} \quad (3)$$

$$\mu_{HS\pm} = \mu_1 + \frac{f_2}{(\mu_2 - \mu_1)^{-1} + \frac{2f_1(K_1 + 2\mu_1)}{5\mu_1 \left(K_1 + \frac{4}{3} \mu_1 \right)}} \quad (4)$$

where,

K_{HS}, μ_{HS} = bulk and shear moduli calculated using Hashin-Strikman bounds;

K, μ = bulk and shear mineral moduli of different constituents (index refers to individual phase 1 or 2);

f = volume fraction of individual phases.

The upper bound is usually used for cemented rocks (stiffest material is subscribed 1), and the lower bound for unconsolidated sands (softest material is subscribed 1). For the modeling purposes in this work a modified Hashin-Shtrikman lower bound has been used. It connects two end members (high porosity and zero porosity) in the porosity-moduli plane (Dvorkin *et al.*, 1996):

$$K_{dry} = \left[\frac{\Phi / \Phi_c}{K_{HM} + \frac{4}{3} \mu_{HM}} + \frac{1 - \Phi / \Phi_c}{K + \frac{4}{3} \mu_{HM}} \right]^{-1} - \frac{4}{3} \mu_{HM} \quad (5)$$

$$\mu_{dry} = \left[\frac{\Phi / \Phi_c}{\mu_{HM} + \frac{\mu_{HM}}{6} \left(\frac{9K_{HM} + 8\mu_{HM}}{K_{HM} + 2\mu_{HM}} \right)} + \frac{1 - \Phi / \Phi_c}{\mu + \frac{\mu_{HM}}{6} \left(\frac{9K_{HM} + 8\mu_{HM}}{K_{HM} + 2\mu_{HM}} \right)} \right]^{-1} - \frac{\mu_{HM}}{6} \left(\frac{9K_{HM} + 8\mu_{HM}}{K_{HM} + 2\mu_{HM}} \right), \quad (6)$$

where,

K_{dry} , μ_{dry} = effective “dry” bulk and shear modulus;

Φ = porosity.

2.1.3 Gassmann fluid substitution

To be able to compare the theoretically modeled results with *in situ* data (logged density, velocities and moduli), fluid substitution has been applied. Fluid substitution is a prediction of fluid saturation effects on seismic properties. It uses Gassmann's equation to calculate elastic properties at the desired saturation, from either the dry rock or a rock saturated with another fluid (Sheriff, 2006). It is remarkably accurate and robust (Mavko *et al.*, 1998) for porosities greater than 10%. Most often, the disagreement between the Gassmann calculations and field measurements can be linked to inappropriate mineral moduli, measurement errors in velocity, density, or porosity, mud-filtrate invasion when working with well logs, *etc.*

Gassmann fluid substitution is used for calculation of elastic properties of clean sands with uniform water saturation for different saturation values, and for porosities from zero to initial/critical porosity, and is expressed as:

$$K_{sat} = K_{dry} + \frac{\left(1 - \frac{K_{dry}}{K_0}\right)^2}{\frac{\phi}{K_f} + \frac{(1 - \phi)}{K_0} + \frac{K_{dry}}{K_0^2}} \quad (7)$$

$$\mu_{sat} = \mu_{dry} \quad (8)$$

where,

K_{dry} = effective bulk modulus of dry rock;

K_{sat} = effective bulk modulus of rock with pore fluid;

K_{min} = effective bulk modulus of mineral material making the rock;

K_{fl} = effective bulk modulus of pore fluid;

μ_{dry} = effective shear modulus of dry rock;

μ_{sat} = effective shear modulus of rock with pore fluid;

Φ = porosity.

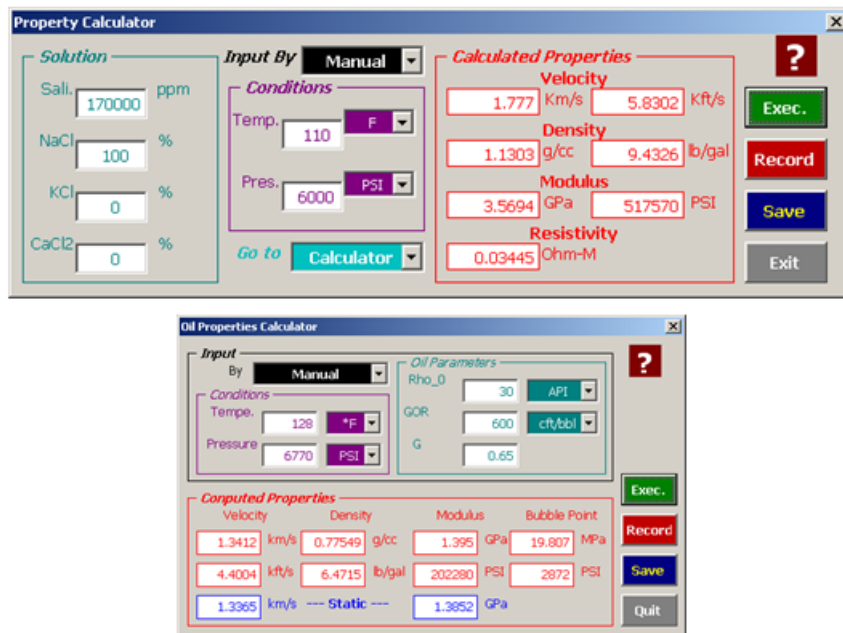


Figure 4. Estimated bulk modulus and density of oil and brine (FLAG program).

The density and bulk modulus of water are functions of temperature, pressure, and salinity. The properties of hydrocarbons, oil, and gas, are more variable and depend strongly on temperature, pressure, and composition (Murphy, 1993). Program FLAG 2008 (based on Batzle and Wang, 1992) has been used to recalculate fluid properties to reservoir condition. According to Hoover MDT data, formation pressure is about 6770 psia, and reservoir temperature 130°F (oil zone, Pleistocene age, at measured depth

12792 – 12895 ft / 3988 – 3930 m). Estimated properties are: oil density $\rho_{oil}=0.77$ g/cc, oil bulk modulus $K_{oil}=1.39$ GPa (Figure 4), water density $\rho_w=1.13$ g/cc and water bulk modulus $K_w=3.56$ GPa, with the water interval at approximately 11870 ft (3923 m).

Fluid density (ρ_{fl}) is a mixture of fluids weighted by saturation - the amount of pore space filled with particular fluid type, and it is defined using equation:

$$\rho_{fl} = S_w \rho_w + (1 - S_w) \rho_{hc} \quad (9)$$

where,

S_w = water saturation in decimal fraction;

ρ_w = density of formation water;

ρ_{hc} = density of hydrocarbon.

The fluid modulus is given by Wood's equation:

$$K_{fl} = \left(\frac{S_w}{K_w} + \frac{(1 - S_w)}{K_{hc}} \right)^{-1} , \quad (10)$$

where,

K_w and K_{hc} = bulk modulus of brine and hydrocarbon, respectively;

S_w = water saturation.

The mass balance equation is used to calculate the bulk density of the rock as a function of porosity and mixed fluids:

$$\rho_b = \rho_g(1 - \phi) + \rho_{fl}\phi , \quad (11)$$

where,

ρ_b = bulk density of the formation;

ρ_g = density of the grains comprising the formation (sand grain density 2.65 g/cc);

ρ_f = density of fluid;

Φ = porosity.

The compressional (V_p) and shear velocity (V_s) are calculated for the new/desired saturation using the following equations:

$$V_p = \sqrt{\frac{K_{sat} + \mu}{\rho_b}} \quad (12)$$

$$V_s = \sqrt{\frac{\mu}{\rho_b}} \quad (13)$$

Gassmann theory includes several assumptions (Wang, 2001). The rock is macroscopically homogeneous and monomineralic. All the pores are communicating (pressure is able to equilibrate, which relates to zero frequency assumption). The pores are filled with frictionless fluid (the viscosity of the saturating fluid is zero). The rock-fluid system is closed (undrained). There is no interaction between solid and fluid (no hardening or softening the frame due to interactions with fluid).

2.1.4 Model results

Based on previously described methodology, the moduli and velocities for the porosity range from 0 to 36%, and water saturation for 15 – 100% were calculated, for both “dry” and “saturated” condition. A fully saturated water zone is represented with $S_w=100\%$, and fully-saturated oil zone with $S_w=15\%$ (*in situ* irreducible water saturation).

All the parameters values are used to best represent the unconsolidated Hoover reservoir and surrounding water zone. Input parameters for modeling “dry” properties represent the following physical quantities: coordination number $n=9$, critical porosity $\Phi_c=0.40$, mineral bulk modulus $K_0=37$ GPa, mineral shear modulus $\mu_0=38$ GPa, Poisson’s ratio for solid phase $\nu=0.08$, effective pressure $P_{eff}=22$ MPa (Appendix II). These are the input parameters in Eq. 1–6. Values used for fluid properties are: $\rho_{oil}=0.77$ g/cc, $K_{oil}=1.39$ GPa, $\rho_w=1.13$ g/cc and $K_w=3.56$ GPa (for water salinity of 170,000 ppm).

The results are plotted as “dry” moduli vs. porosity (Figure 5), “dry” bulk vs. “dry” shear modulus (Figure 6) and “dry” velocities (V_p and V_s) vs. porosity (Figure 7). End-member bulk modulus calculated using Hertz-Mindlin theory is 1.91 GPa, and shear modulus 2.80 GPa (for initial porosity equal 36%). This is usually rigid for such a compressible rock.

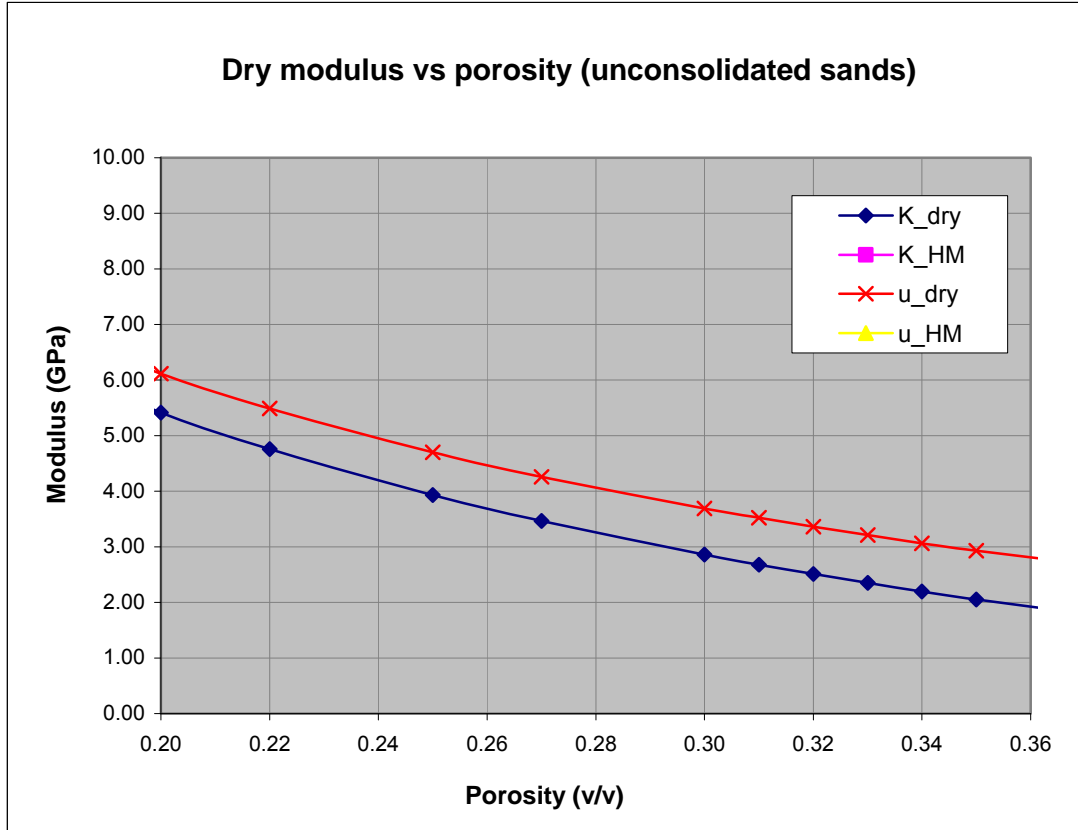


Figure 5. Theoretically predicted “dry” bulk and shear moduli as a function of porosity for sandstones with porosity ranging from 0.20 to 0.36 ($P_{\text{eff}} = 22$ MPa).

The ratio between predicted “dry” shear and bulk modulus is 1.02 at low porosities, and increases in high porosity range up to 1.40. The expected ratio should be constant (close to 1), and approximately the same as the ratio of mineral moduli. This is one of indication of shear modulus being overpredicted by Hertz-Mindlin theory, especially for high porosities.

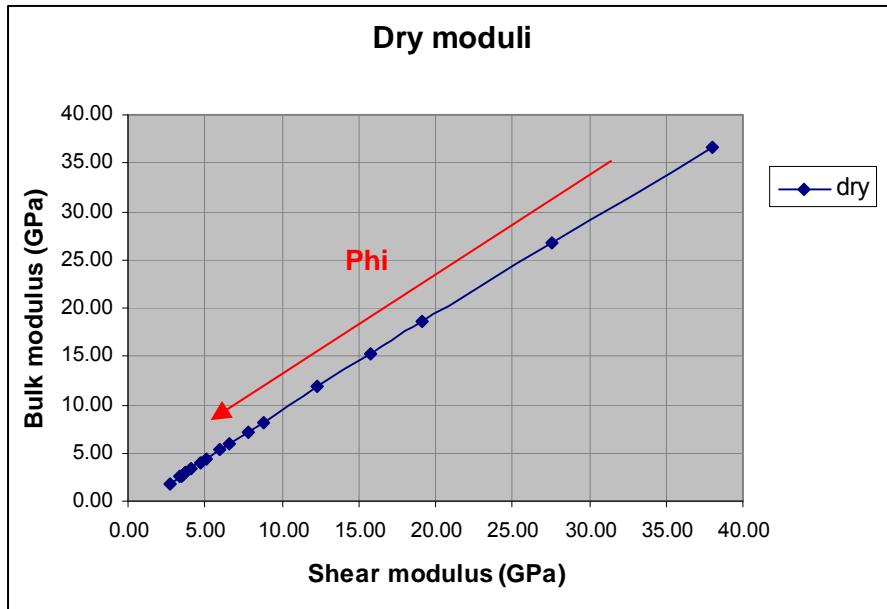


Figure 6. Theoretically predicted “dry” bulk vs. shear modulus. Red curve indicates the direction of porosity decrease.

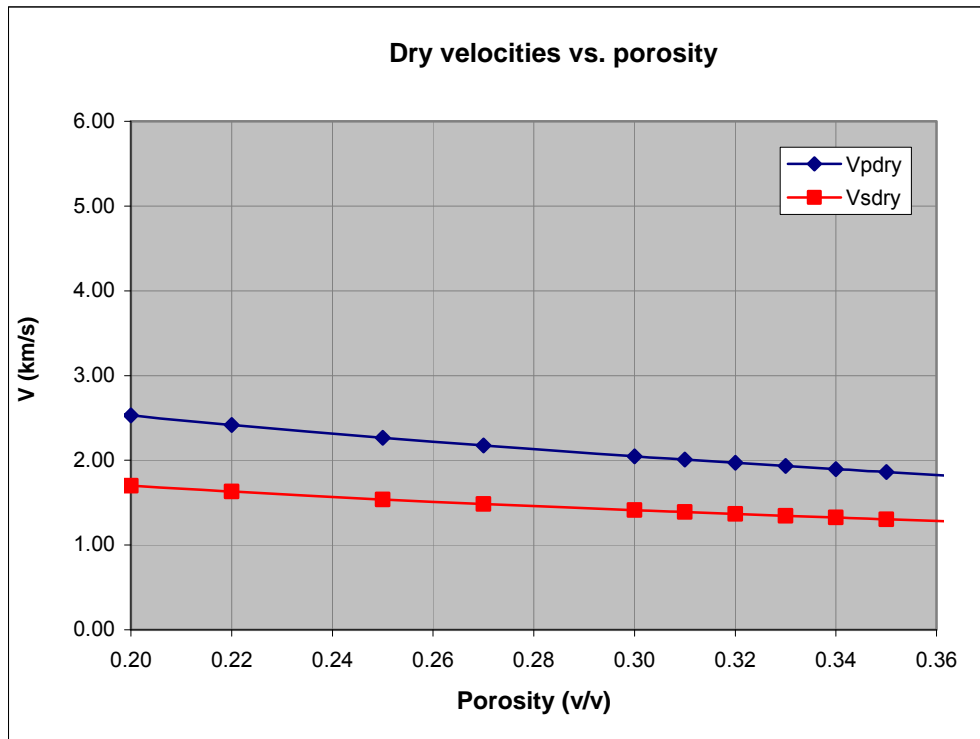


Figure 7. Theoretically predicted “dry” P-wave and S-wave velocities as a function of porosity for sandstones with porosity ranging from 0.20 to 0.36 ($P_{\text{eff}} = 22 \text{ MPa}$).

On the other hand, the theory gives good prediction for bulk modulus (Figure 8). Thus P-wave velocity will suffer only from error generated through wrong shear modulus and be slightly overpredicted (percentage error for oil sand: 4.0%, and for wet sand: 3.6%; Figure 9). S-wave velocity will incorporate much larger error and be highly overpredicted (percentage error for oil sand: 20.2%, and for wet sand: 18.6%).

The criteria for “good” or “bad” fit are based on ability to reconstruct *in situ* measurements. In our case, fluid substitution was performed on theoretical model results and compared with logged data. The initial assumption is that if well log data points fall close to a theoretical line in velocity-porosity or modulus-porosity plane, then internal structure of a rock is similar to the idealized structure predicted by theoretical model.

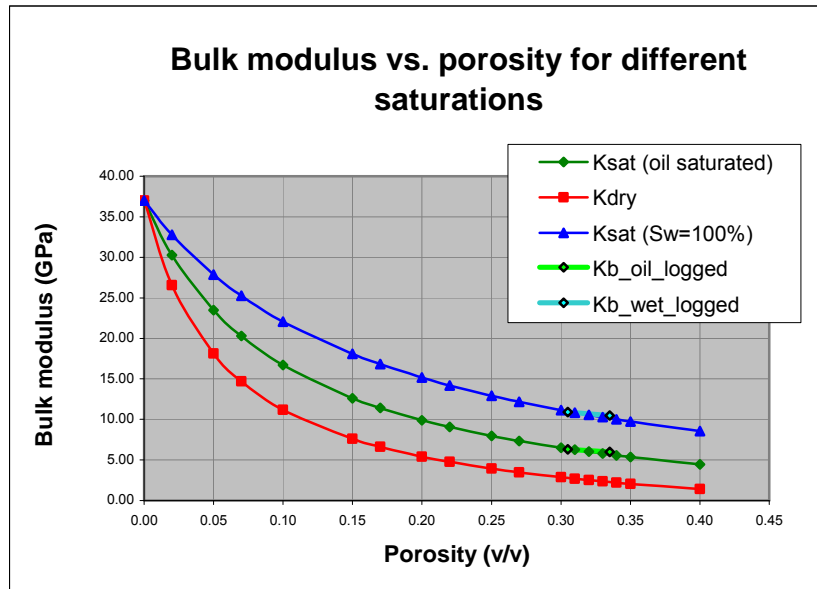


Figure 8. Theoretically predicted bulk modulus for different water saturation: oil saturated case (dark green trend line), water-saturated case (dark blue line) and for dry case (red line). Logged data trend lines superimposed for the porosity 30.5-33.5% (light green and light blue trend lines for oil and wet sand, respectively).

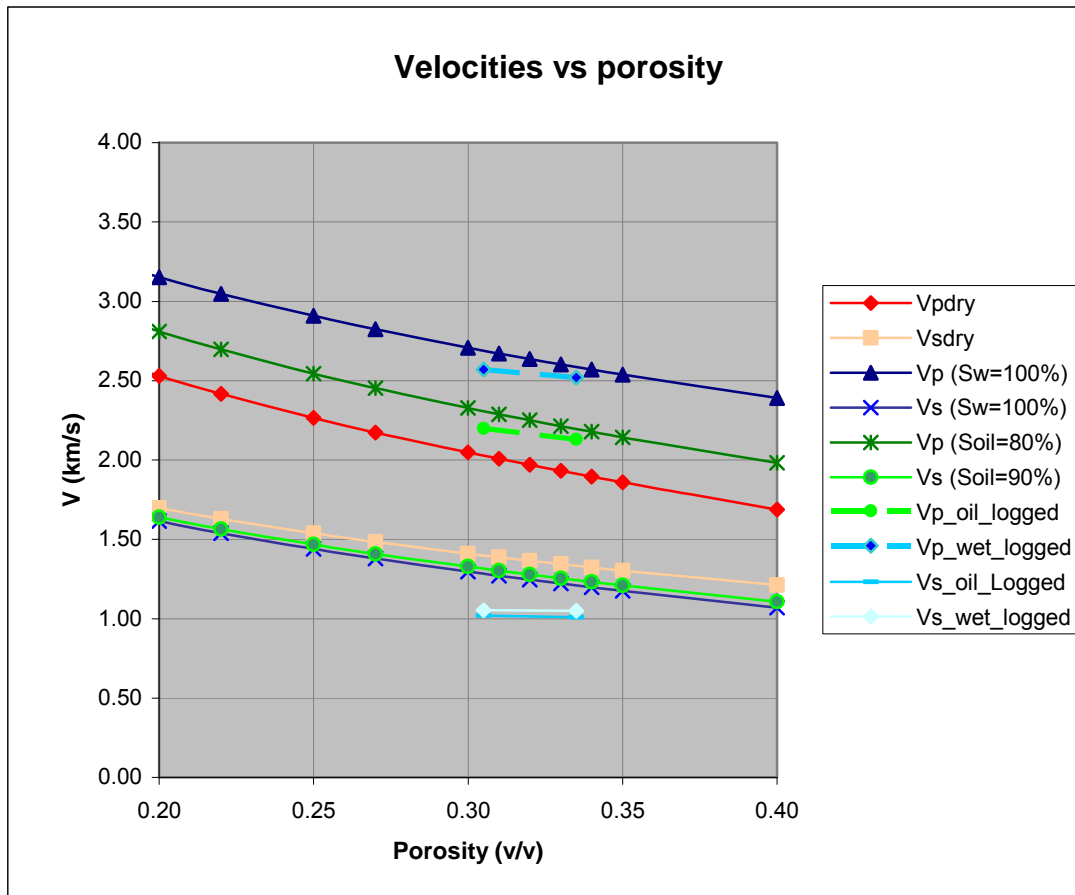


Figure 9. Theoretically predicted P- and S-wave velocities as a function of porosity for wet, oil and dry case ($P_{eff} = 22$ MPa). Superimposed: logged data for the porosity 30.5-33.5% (light green and light blue trend lines for oil and wet sand, respectively).

S-wave velocity being overpredicted will result in underpredicted V_p/V_s ratio. Figure 10, shows that predicted V_p/V_s for high porosity sand is 2.2-2.25 for wet sands, which is lower than observed 2.5-2.55 on logged data. Oil sands exhibit also underpredicted values of 1.8-1.9 compared with logged 2.1-2.2.

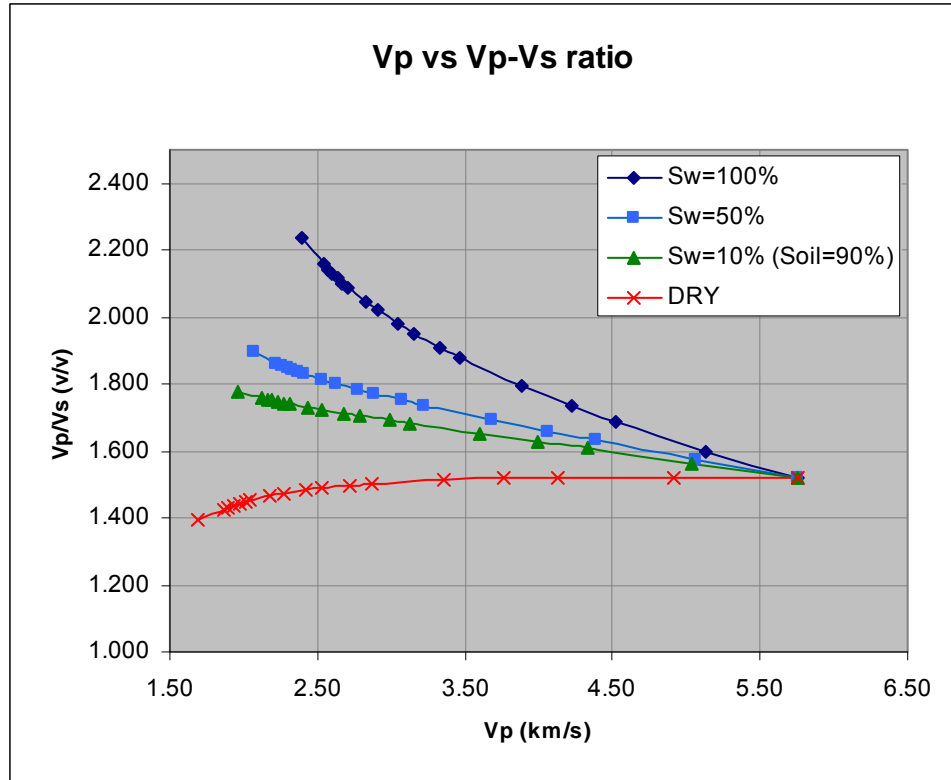


Figure 10. Theoretically predicted V_p/V_s vs. V_p velocities ($P_{eff} = 22$ MPa).

After correcting for slip factor, new V_p , V_s and V_p/V_s are obtained. Corrected bulk and shear modulus are presented in Figure 11. Compared with bulk and shear modulus trend line for Ottawa and Troll sand ultrasonic measurements (Blangy, 1992) they exhibit similar behavior, though having a narrower range and remaining within the range of Blangy's trends (Figure 12).

Percentage error for corrected P-wave velocities in oil sand is now 1.16%, and for wet sand 1.0% (Figure 13). S-wave velocity are reduced, and percentage error for oil sand is 3.9%, and for wet sand 3.2%.

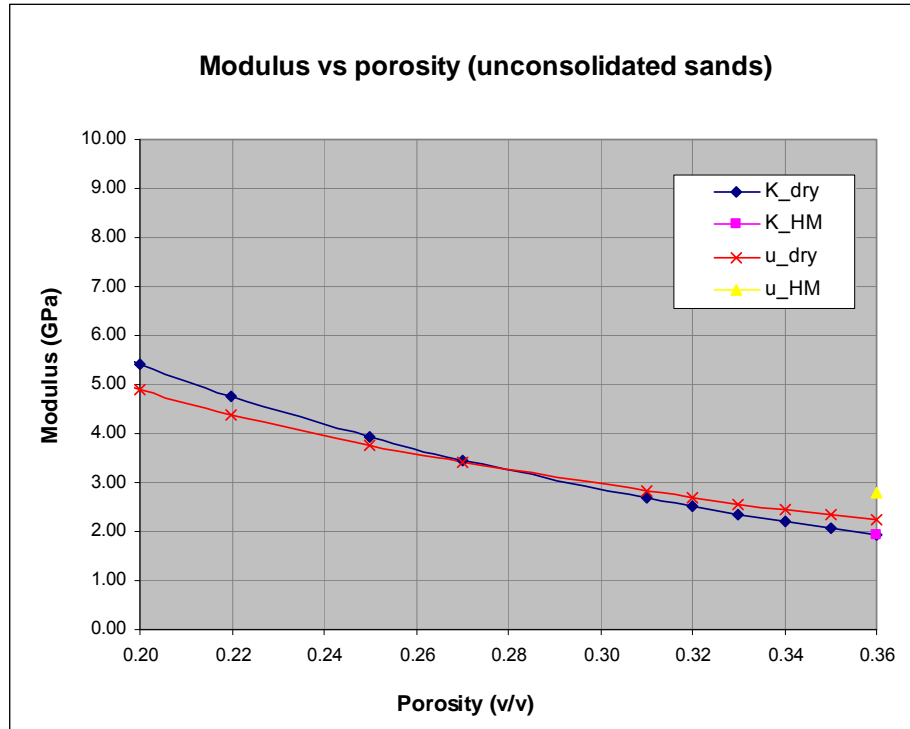


Figure 11. Moduli after slip-factor correction (shear modulus reduced).

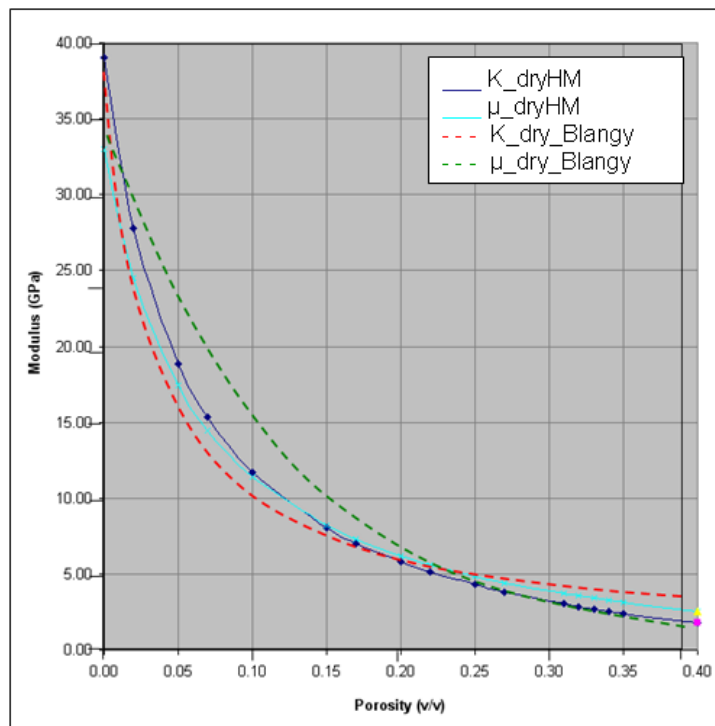


Figure 12. Slip-corrected moduli superimposed with Ottawa and Troll sands (Blangy, 1992) in modulus vs. porosity plane.

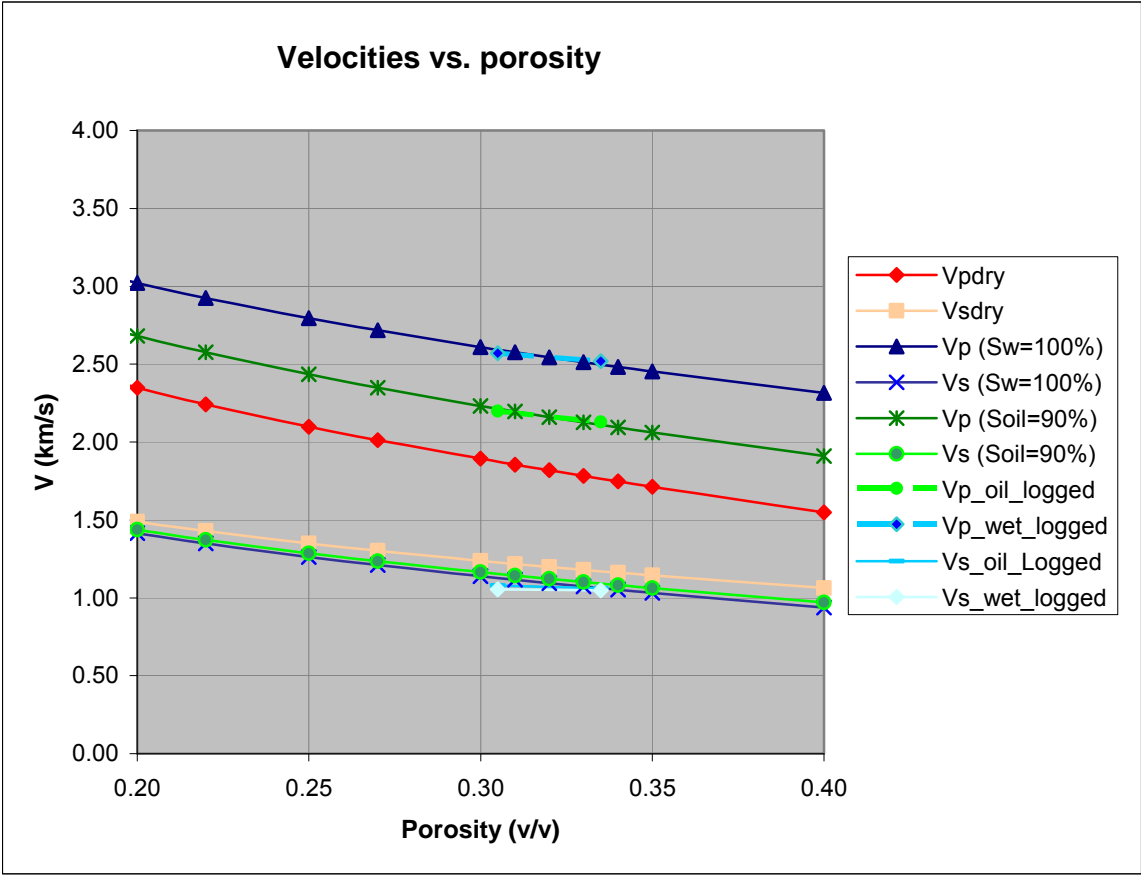


Figure 13. Theoretically predicted P- and S-wave velocities after slip-factor correction, superimposed with logged data for the range 30.5-33.5% porosity.

It can be observed, that the velocity separation between oil- and water-saturated conditions beyond the consolidation porosity, which is around 30% (depending on sand sorting) grows with porosity reaching 35%. This separation has been reported for gas saturated vs. brine saturated rock and used in AVO analysis. From our example, we conclude that it is also possible to distinguish a live oil reservoir from an aquifer, especially in the case of high salinity brine. The higher the contrast in fluid properties, both densities and velocities will differentiate more.

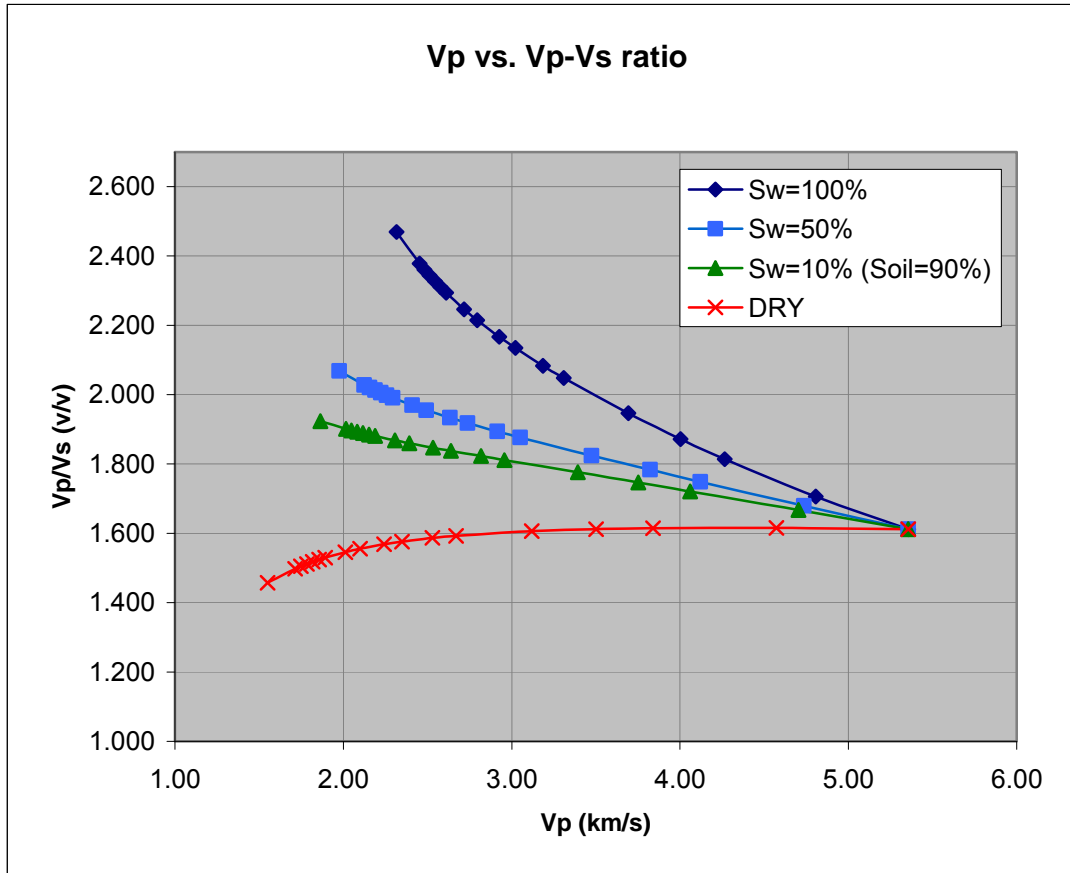


Figure 14. Theoretically predicted V_p/V_s ratio after slip-factor correction.

2.2 Heuristic models

In this section the linear critical porosity model (Nur, 1992) and the nonlinear model by Krief et al. (1990) are compared. Both incorporate two elements: (1) establish empirical relations between V_p , V_s , and porosity for each lithology, referring to a single fluid (usually water), and (2) use Gassmann's equation to recalculate elastic properties to other pore fluid states.

2.2.1 Critical porosity model

A general expectation is that the velocities of rocks, as well as their V_p/V_s ratios, should trend toward the value for the solid mineral material, in the low porosity range, and toward the value for a fluid suspension at some limiting high porosity (Castagna *et al.*, 1993). The critical porosity model (CPM) describes different velocity-porosity relationships below and above the characteristic porosity point (critical porosity).

In the suspension domain, the effective bulk (K_{sat}) and shear moduli (μ_{sat}) of the rock can be estimated using the Reuss bound (Mavko *et al.*, 1998):

$$\frac{1}{K_{sat}} = \frac{\phi}{K_{fl}} + \frac{1-\phi}{K_0} \quad (14)$$

$$\mu = 0 \quad (15)$$

where K_{fl} and K_0 are the bulk moduli of the fluid and mineral and Φ is the porosity.

In the load-bearing domain, the moduli increase from the suspension values at critical porosity toward the mineral values at zero porosity. When expressed as modulus versus porosity, this trend can be approximated with a straight line (Nur, 1992; Nur *et al.*, 1995). For dry rocks (*i.e.*, rocks with infinitely compressible pore fluid), the bulk and shear moduli can be expressed as linear functions:

$$K_{dry} = K_0 \left(1 - \frac{\phi}{\phi_c}\right) \quad (16)$$

$$\mu_{dry} = \mu_0 \left(1 - \frac{\phi}{\phi_c}\right), \quad (17)$$

where, K_0 and G_0 are the mineral bulk and shear moduli. Gassmann equation is used to calculate moduli at saturation condition from “dry” properties.

Expected critical porosity value is different for different classes of rocks. Listed are some critical porosity values (in p.u.) of porous materials from Nur *et al.* (1995):

Cracked Rocks:	0.005 - 0.01
Oceanic Basalt:	0.05 - 0.01
Limestone:	0.30 - 0.35
Dolomites:	0.30 - 0.35
Sandstones:	0.35 - 0.40
Chalks:	0.55 - 0.65
Volcanic Glass:	0.90

2.2.2 Krief model

Krief's equation is a nonlinear form that results from fitting a single function to the two domains, below and above critical porosity. Krief *et al.* (1990) suggest modeling of a dry rock as porous elastic solid, where the dry rock bulk modulus is a function of mineral moduli and Biot's coefficient. Using the sandstone data of Raymer *et al.* (1980), they defined an empirical relation for Biot's coefficient and porosity, so that the dry modulus is given by following equations:

$$K_{dry} = K_0(1 - \phi)^{m(\phi)} \quad (18)$$

$$\mu_{dry} = \mu_0(1 - \phi)^{m(\phi)}, \quad (19)$$

where $m(\phi) = 3/(1 - \phi)$.

2.2.3 Model results

Synthetic responses of elastic properties, for both dry and saturated conditions, are generated for porosity range from 0 to 40% using the Critical porosity model and Krief's model. The reported critical porosity value for sandstones ranges between 35 and 40%, thus two cases are investigated: the critical porosity model with $\Phi_c=40\%$ (labeled as CRITSYNT_PC40) and the critical porosity model with $\Phi_c=36\%$ (labeled as CRITSYNT_PC36). Krief's model results are marked as KRIEF_SYNT.

Used input parameters are: $K_0=37$ GPa, $\mu_0=38$ GPa, $K_w=3.56$ GPa, $K_{oil}= 1.39$ GPa, $\rho_q=2.65$ g/cc, $\rho_w=1.13$ g/cc, $\rho_{oil}=0.77$ g/cc, $S_w=15-85\%$, $\Phi=0-40\%$.

The comparison between the models in modulus vs. porosity plane is shown in figure 15. One can observe a similar, almost identical, behavior of Krief dry bulk modulus ($K_{dry_KRIEFSYNT}$) and CPM dry bulk modulus for $\Phi_c=36\%$ ($K_{dry_CRITSYNT_PC36}$) in the range of low porosities up to 25%. After that point, moduli greatly diverge and Krief's bulk modulus becomes more similar to CPM bulk modulus for $\Phi_c=40\%$ ($K_{dry_CRITSYNT_PC40}$).

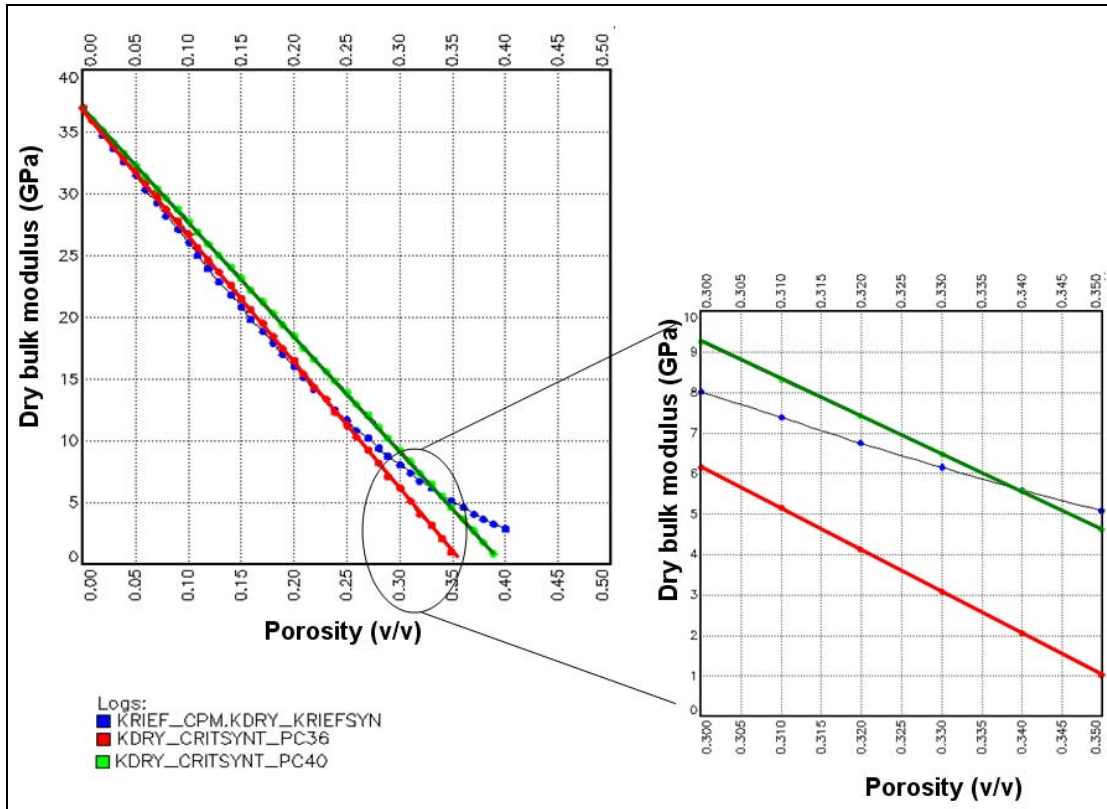


Figure 15. Dry bulk modulus vs. porosity: Krief and Critical porosity model.

Zooming into the porosity range of 30-35% (Figure 14- right), we can notice large variation in $K_{dry_CRITSYNT_PC36}$, ranging from 6.1-1.0 GPa, and more subtle change in other two models results: $K_{dry_CRITSYNT_PC40}$ from 9.2-4.7 GPa, and $K_{dry_KRIEFSYNT}$ from 8.0-5.0 GPa. If we consider that bulk modulus calculated from logged data in oil zones is about 5.9 GPa, and in water zone about 11.0 GPa, (averaged for high porosity range, Figure 16), the moduli calculated using these two heuristic models seems too stiff and can not reproduce actual *in situ* velocities. CPM with $\Phi_c=36\%$ gives relatively better results, while CPM with $\Phi_c=40\%$ is highly overpredicted.

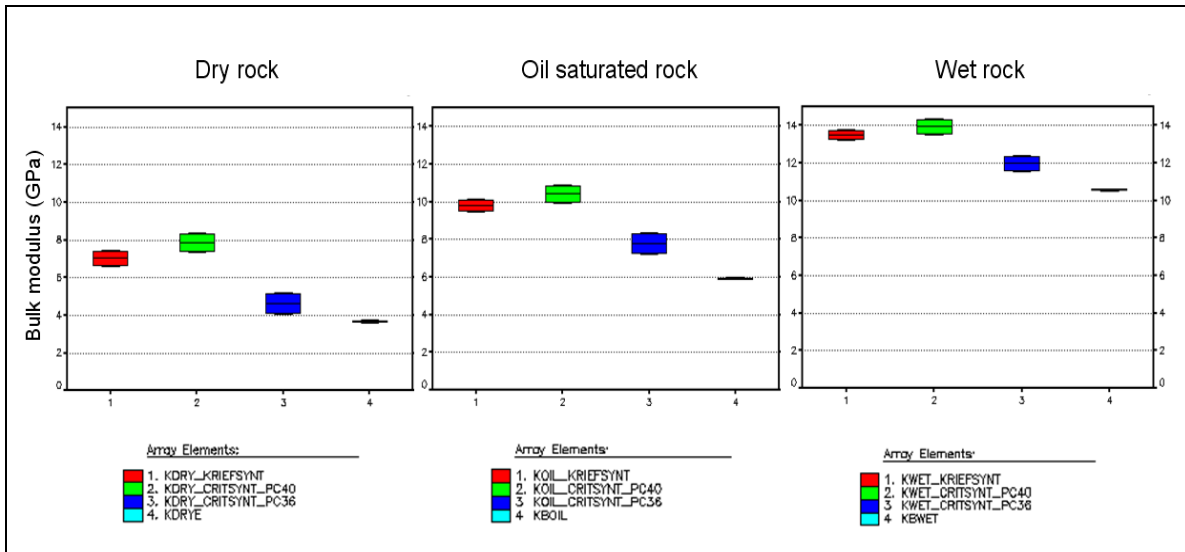


Figure 16. Bulk modulus vs. porosity: Krief, Critical porosity model and logged data comparison: dry (left), oil-saturated (middle), water-saturated (right). Porosity range 31-33%.

Corresponding “dry” velocities are shown in Figure 16. Focusing on high-porosity range (Figure 17), one can observe significant “dry” V_p reduction from 2.8km/s to 1.2 km/s and V_s reduction from 1.8 km/s to 0.8 km/s for CPM ($\Phi_c=36\%$). Krief and

CPM ($\Phi_c=0.40$) are highly overpredicting both V_p and V_s , being in a range of elastic properties for saturated rocks.

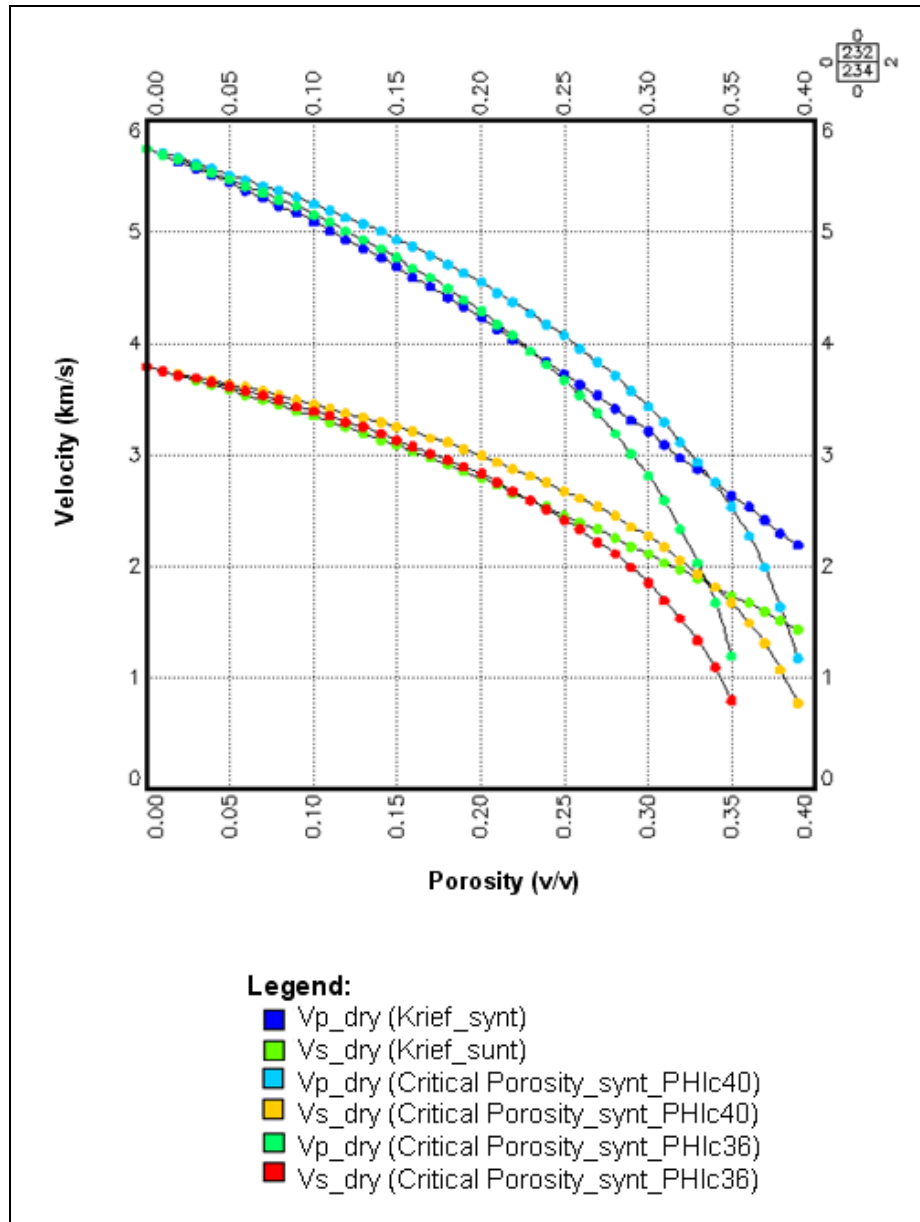


Figure 17. “Dry” P-wave and S-wave velocities vs. porosity: Krief and Critical porosity models.

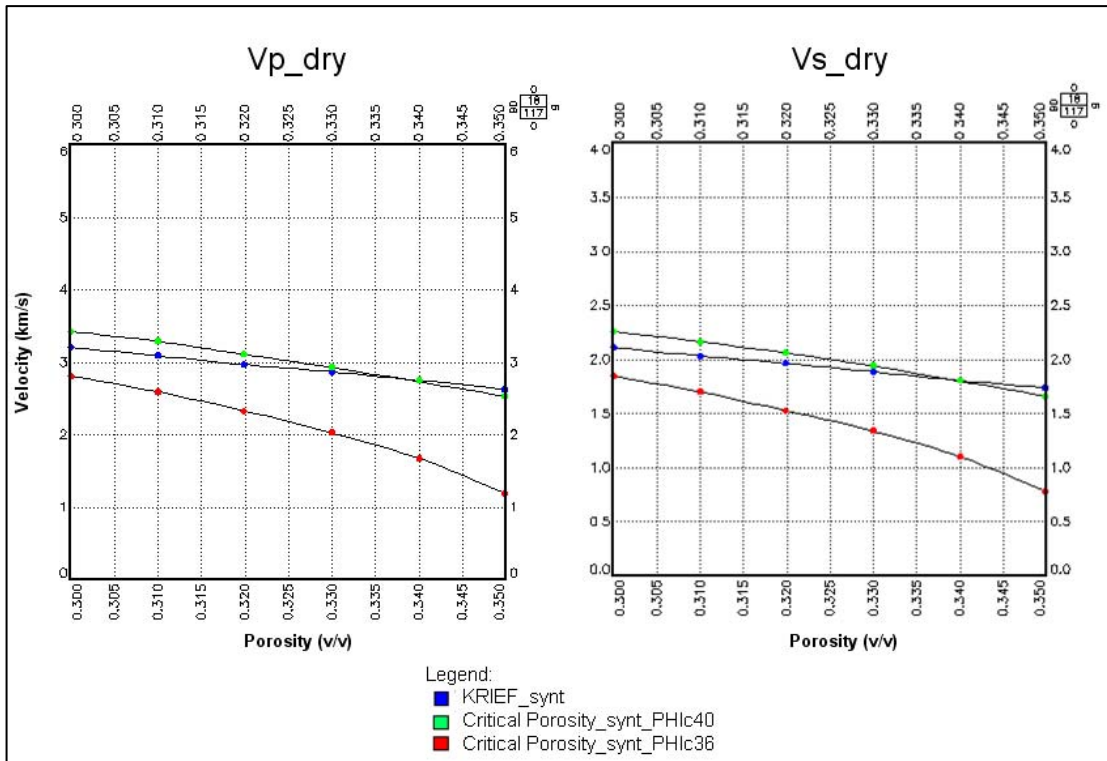


Figure 18. Dry velocity vs. porosity: Krief and Critical porosity model. P-wave (left) and S-wave (right). Porosity range 30-35%.

Compared with logged data, all the models show overpredicted properties for both V_p (Figure 19) and V_s (Figure 20), resembling in acoustic behavior more to compacted rock (upper bound). Comparison has been made for “dry”, oil- and brine-saturated condition.

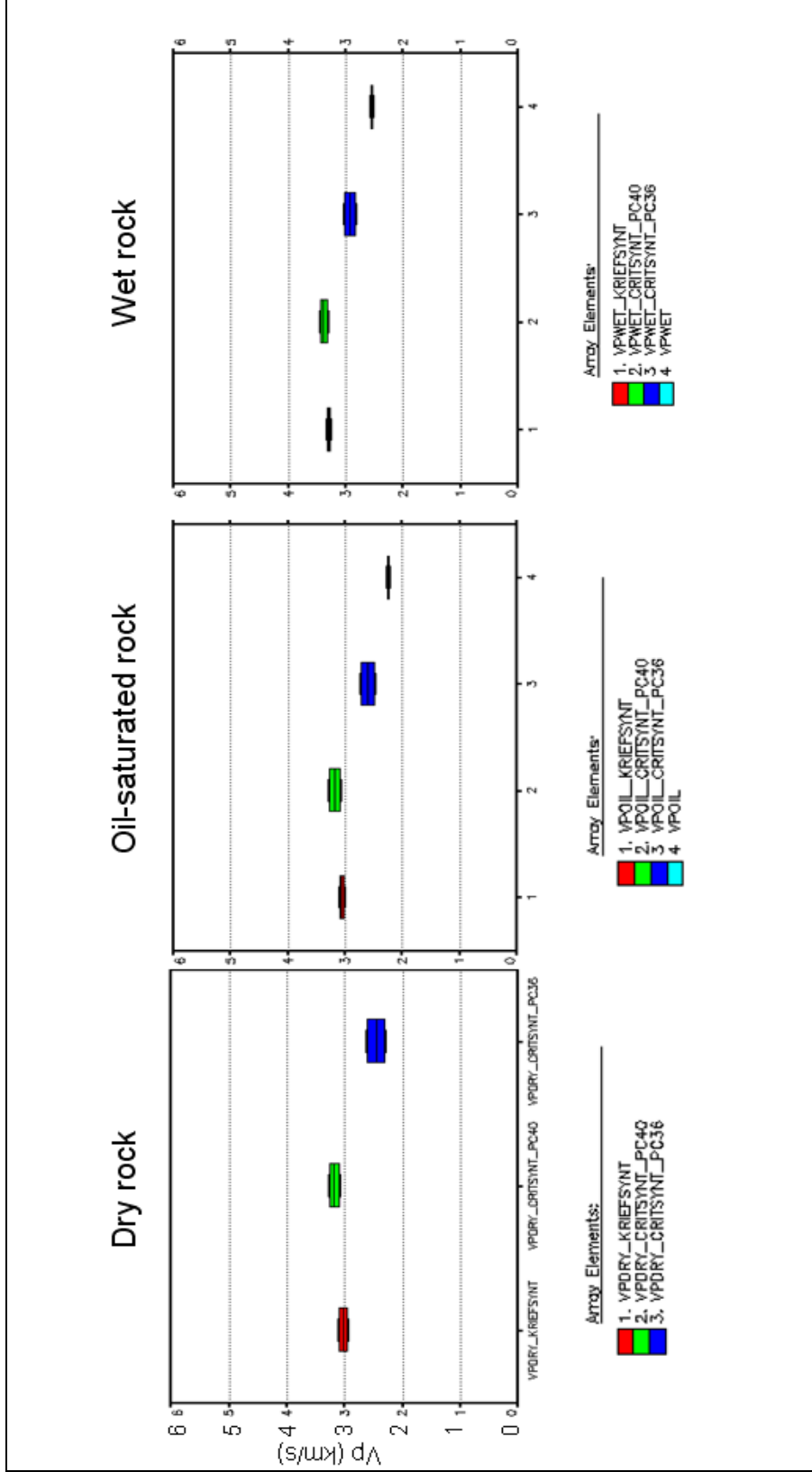


Figure 19: P-wave velocity vs. porosity: Krief, Critical porosity model and logged data comparison: (left) dry, (middle) oil-saturated, (right) water-saturated. Porosity range 31-33%.

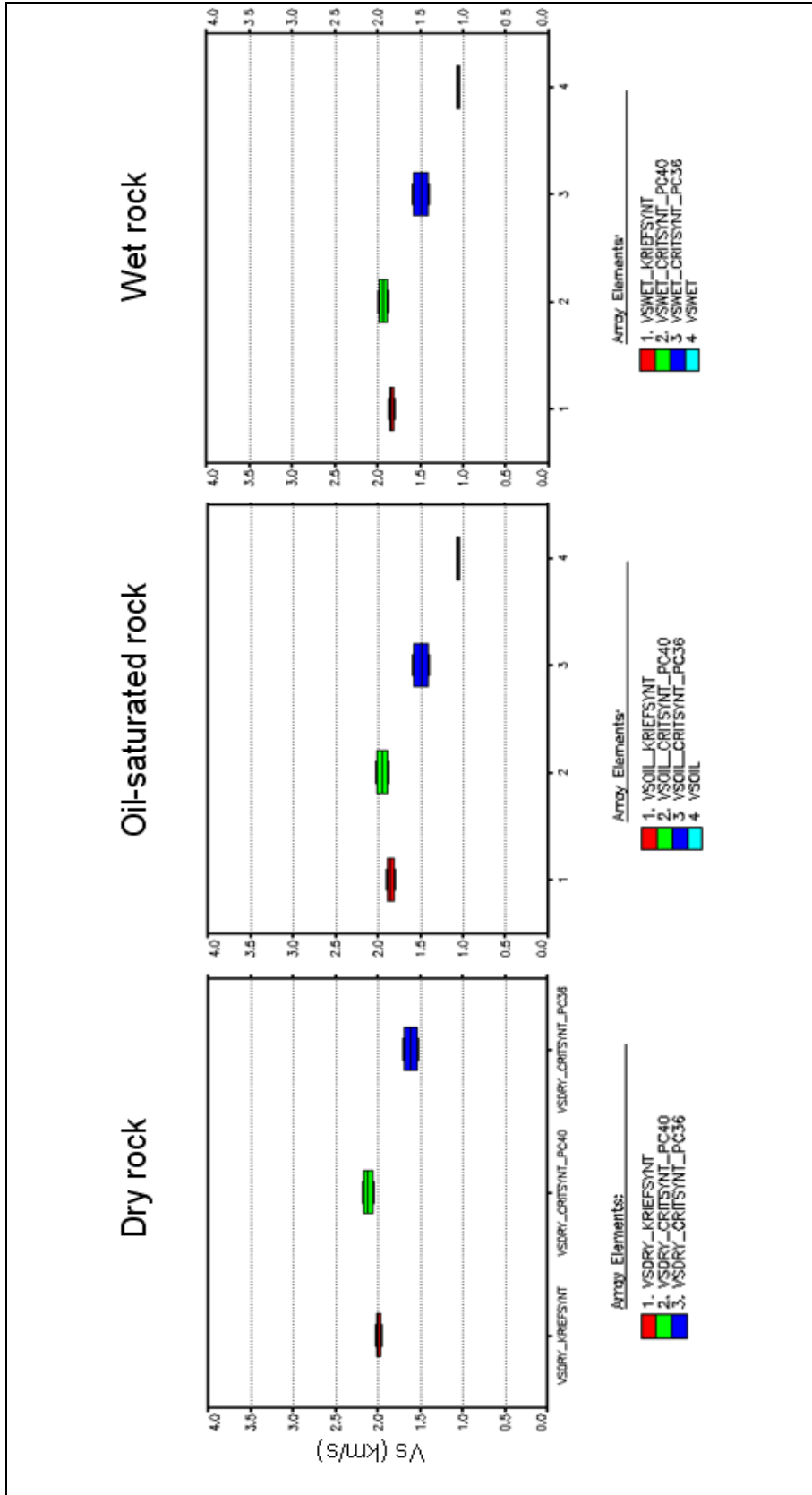


Figure 20: S-wave velocity vs. porosity: Krief, Critical porosity model and logged data comparison: (left) dry, (middle) oil-saturated, (right) water-saturated. Porosity range 31-33%.

3. ELASTIC PROPERTIES: Hoover Field, Gulf of Mexico

3.1 Data set overview: Hoover field, Gulf of Mexico

The Hoover field, discovered in 1997, is located 160 miles south of Galveston, Texas, in deepwater Gulf of Mexico region with water depth of 4800 ft / 1463 m (Figure 21). It is located in the Diana mini-basin, which contains several fields: Hoover, Diana, Diana South, Marshall, and Madison fields (Sullivan *et al.*, 2004). The Hoover field is a low-relief anticline approximately 13,000 ft (3962 m) below sea level, on seismic seen at approximately 4.2 s as a bright spot (Figure 22). The reservoir is low impedance and close to a class III AVO anomaly, but showed the same properties when filled with brine as well (Burtz *et al.*, 2002).

The main reservoir consists of unconsolidated deepwater turbidite deposit, and is Pliocene-aged. The sand channel laterally pinches out against two shale diapirs. Within the reservoir-prone intervals, sheet sandstones, passive shale fills, and mass transport complexes can be defined (Mallarino *et al.*, 2006). Sands are poorly to moderately sorted, and medium-, fine-, and very fine-grained. Most of the sand is massive, however, planar-stratification and ripple cross-stratification occur at the top of some beds. This sand contains fewer lithic fragments and is rich in quartz. Reservoir quality of this sand is excellent due to the well preserved and well interconnected nature of the intergranular pore system. Only minor amounts of clinoptilolite are scattered over framework grain surfaces (Mallarino *et al.*, 2006).

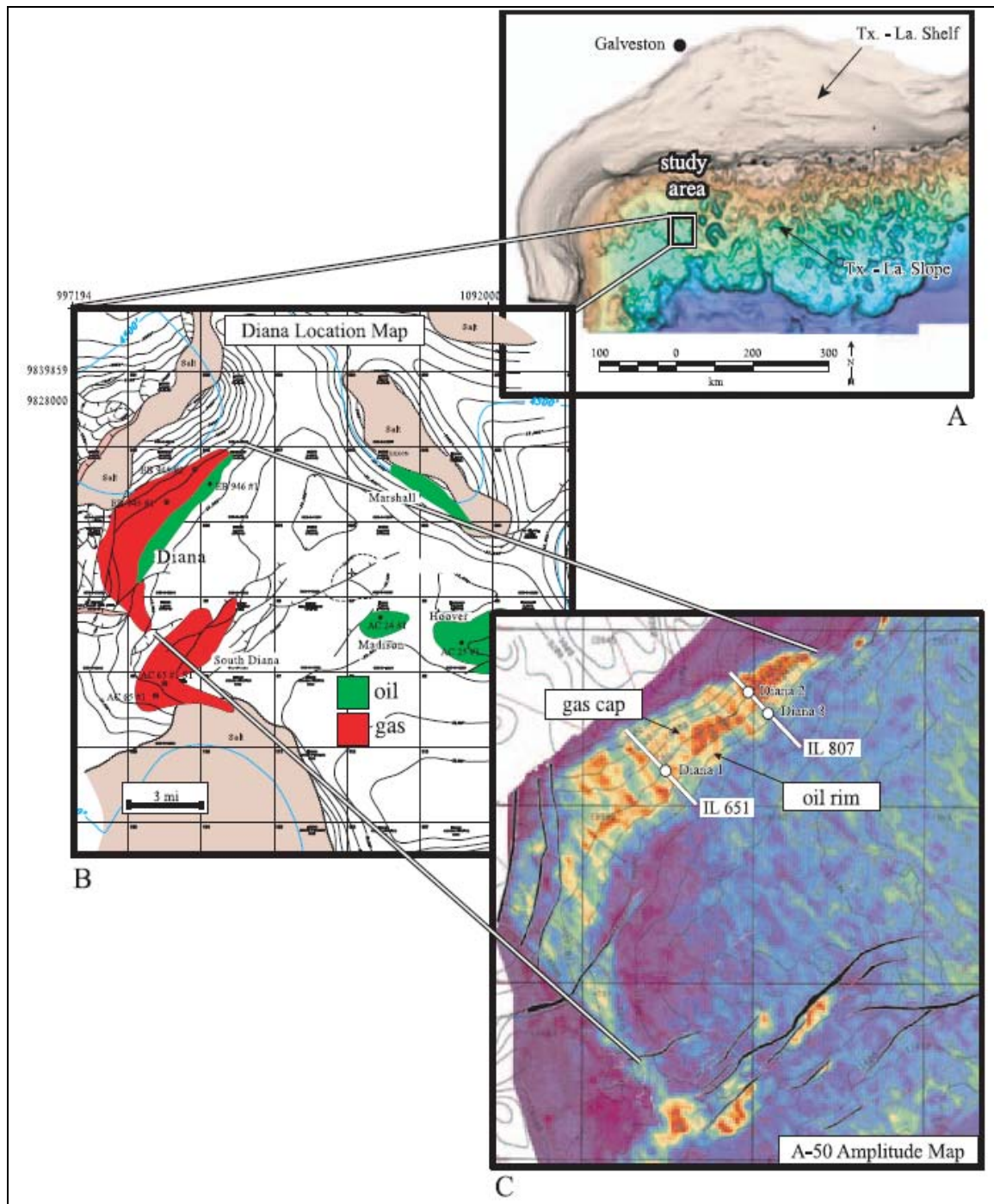


Figure 21. The Diana mini-basin. A) Location: western Gulf of Mexico 255 km south of Galveston. B) Five discoveries: Diana, South Diana, Marshall, Madison and Hoover. C) Combined structure and amplitude extraction for the upper Pliocene A-50 reservoir: high amplitudes are presented as yellow/red colors, and low amplitudes with green/blue colors (Sullivan *et al.*, 2004).

Hoover crude is bio-degraded, with an 30°API oil gravity. The reservoir pressure is about 6770 psia, temperature ~130°F, and it is a water-drive. It is high porosity and high permeability reservoir (the average porosity is about 30%, and the average permeability is about 1.2 Darcies).

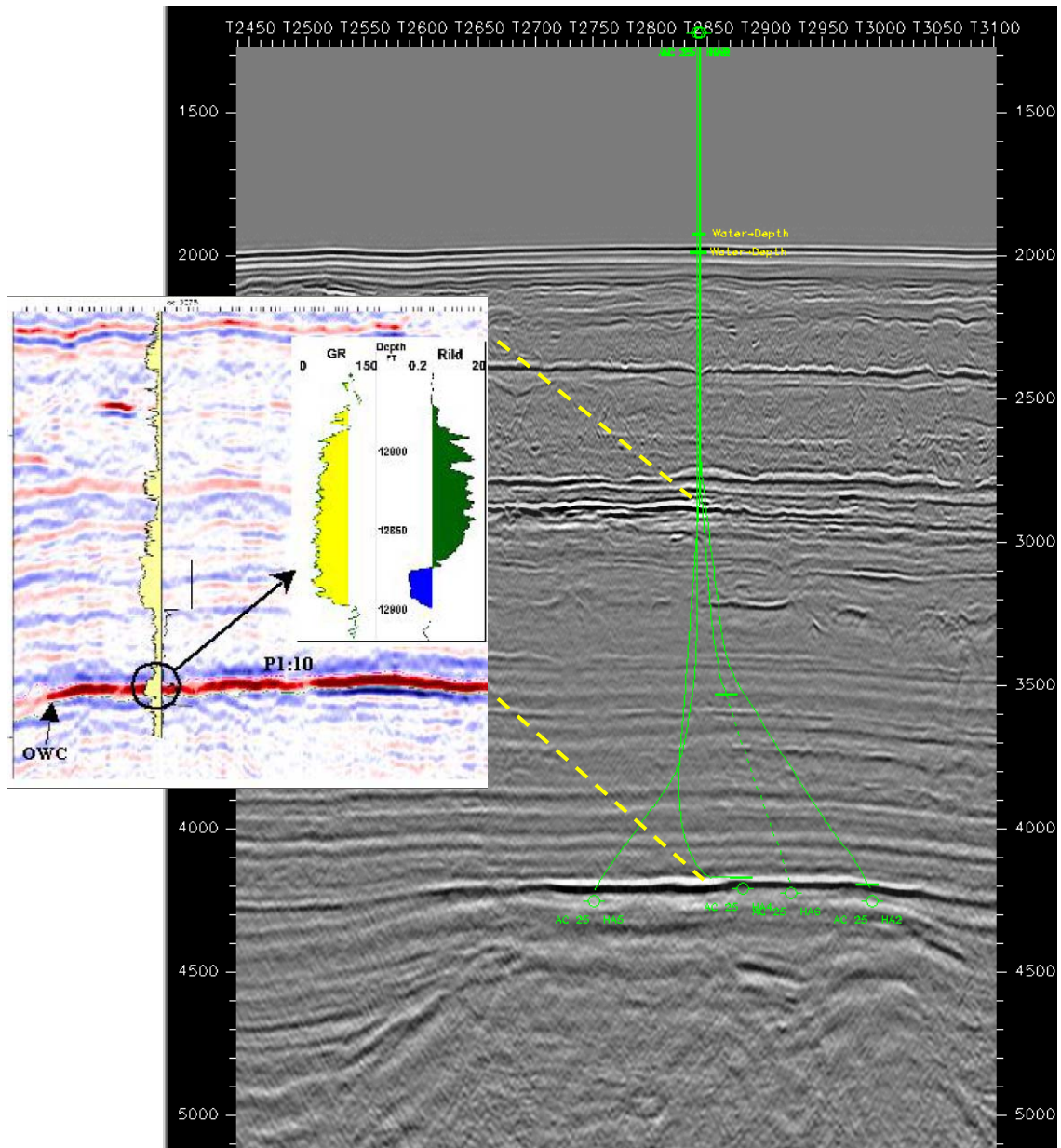


Figure 22. Seismic section at well locations (vertical scale is time, in ms). Seven wells penetrate Hoover oil reservoir, four of which are presented.

3.2 Elastic properties at Hoover field (well log data)

Well log, mudlog, and pressure data are incorporated into the analysis. There are seven wells with regular suite of logs: gamma ray (GR), resistivity, density (RHOB), and neutron porosity (NPHI), three of which had compressional sonic log (DTC), and only one well, Hoover-1, with dipole sonic data (DTS). Hoover-1 is the first drilled well in Hoover with approximately 97 ft (30 m) of pay.

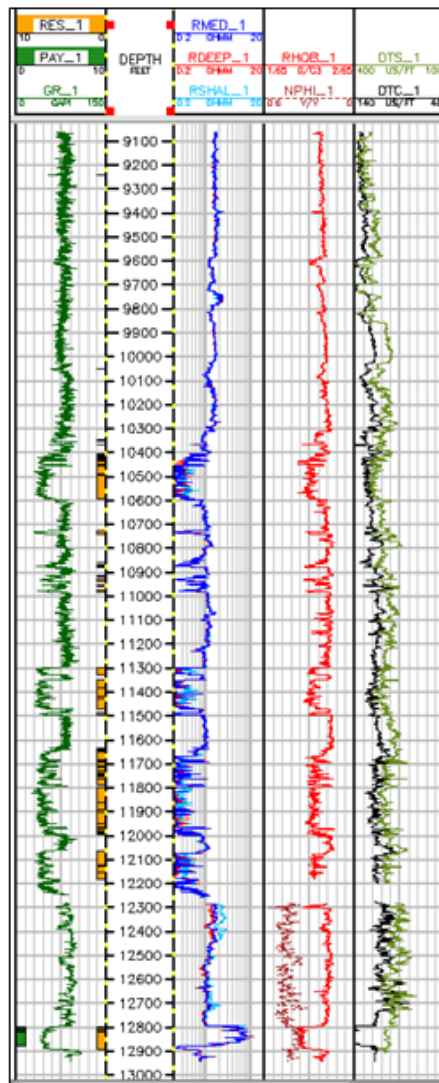


Figure 23. The composite log: Hoover-1. The whole interval logged: 9100-12950 ft (9774-3947 m) MD.

Only well Hoover-1 is considered for detailed rock physics modeling, due to the lack of complete sets of data on other wells. All the other wells were only petrophysically analyzed. Logs were edited for bad data caused by washouts, depth shifts, *etc.* The raw waveforms were not available, so the accuracy of the computed shear and compressional values is taken as given.

The whole logged section consists of shales, several wet sand intervals, and oil zone (Figure 23). There is a small water interval below the oil/water contact. The relationship between elastic properties and porosity in sands and shales is investigated.

In a moduli vs. porosity plane presented in Figure 24, *in situ* data are superimposed with Hashin-Shtrikman upper and lower bounds for clean sand filled with different fluids. The blue line represents the wet sand trend, the green line is the oil sand, and the red is the dry rock. It can be observed that logged data follow lower bound which is expected for high porosity rocks (both sands and shales). In a range of porosity 30-34% oil-sand bulk modulus ranges from 5.0-6.5GPa, wet sand bulk modulus 10.0-12.0 GPa.

In a velocity vs. porosity plane (Figure 25), logged data show large spread. As the whole interval observed is about 3000 ft, different effects are involved: pressure, temperature, compaction, *etc.* The-oil sand velocities are: $V_{p_{\text{mean}}}=2.15$ km/s, $V_{s_{\text{mean}}}=1.2$ km/s; for wet sand $V_p = (2.4-2.7$ km/s), and $V_s = (0.75-1.25$ km/s).

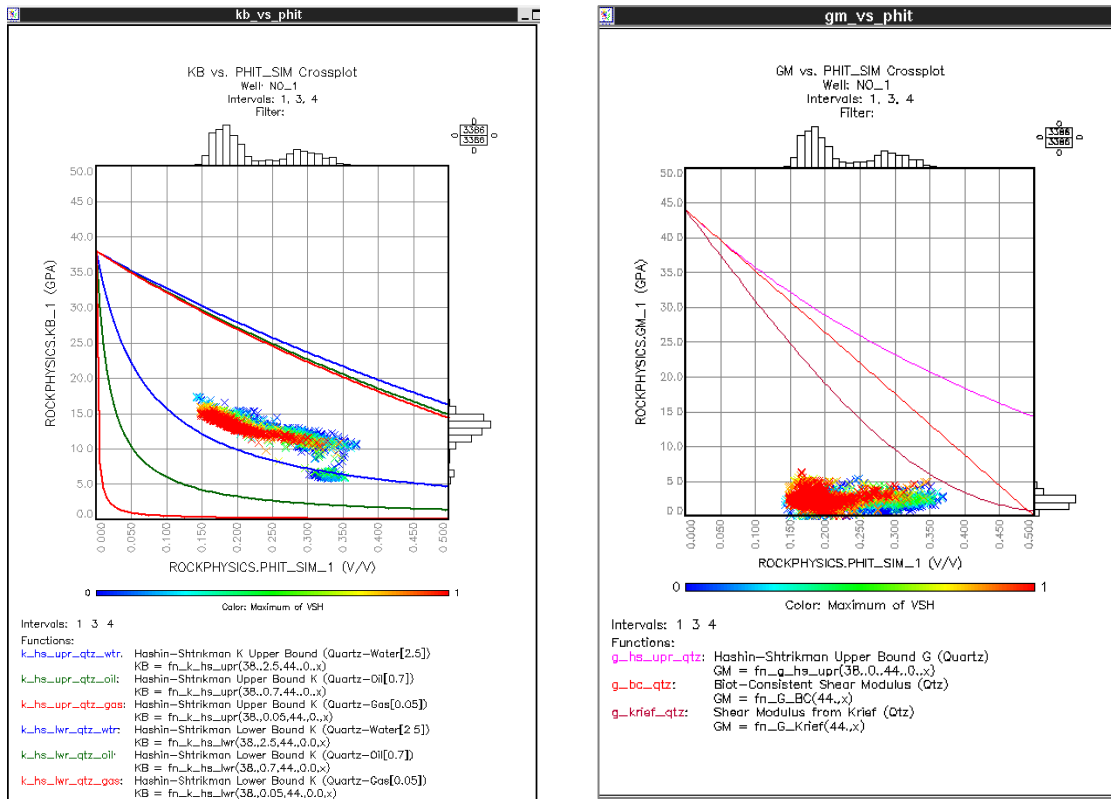


Figure 24. *In situ* moduli vs. porosity: bulk modulus (left) and shear modulus (right).

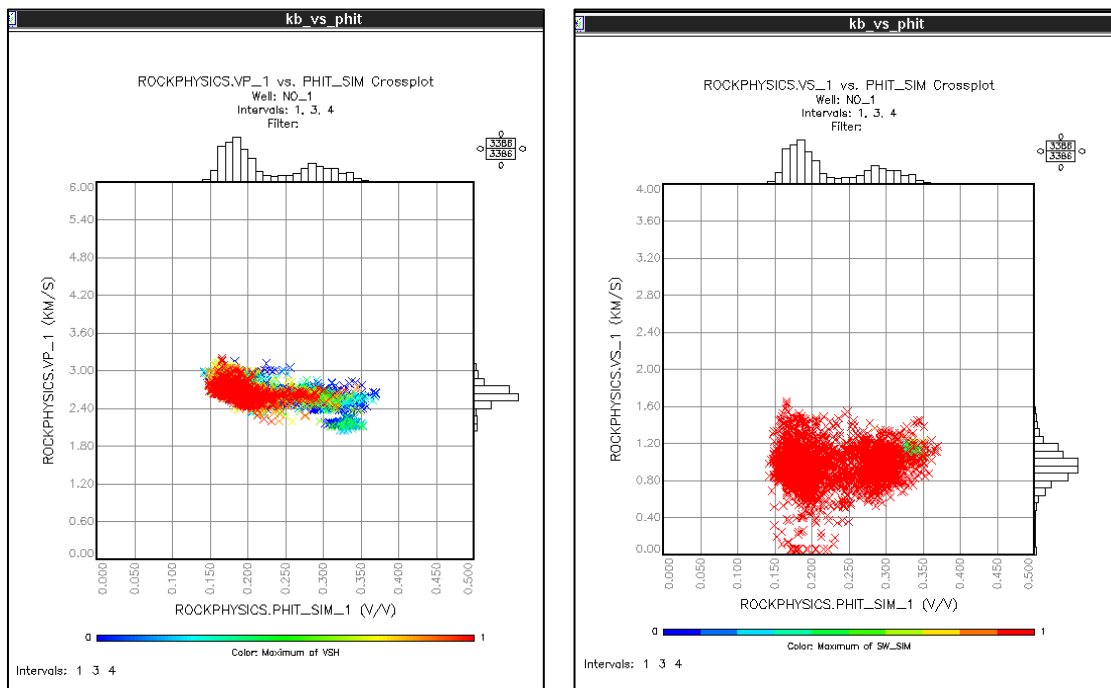


Figure 25. *In situ* velocities vs. porosity: P-wave velocity (left) and S-wave velocity (right). Right figure is color-coded by saturation.

Several observations are made while comparing wet sand and shale velocities:

- 1) Velocities (and densities, as well) vary as a function of depth, primarily due to compaction. Thus, it is reasonable to expect the AVO response of wet sands to also exhibit depth dependence.
- 2) In most of sand–shale pairs, compressional velocities for the shales are 1–15 % faster than those in wet sands (Figure 26).

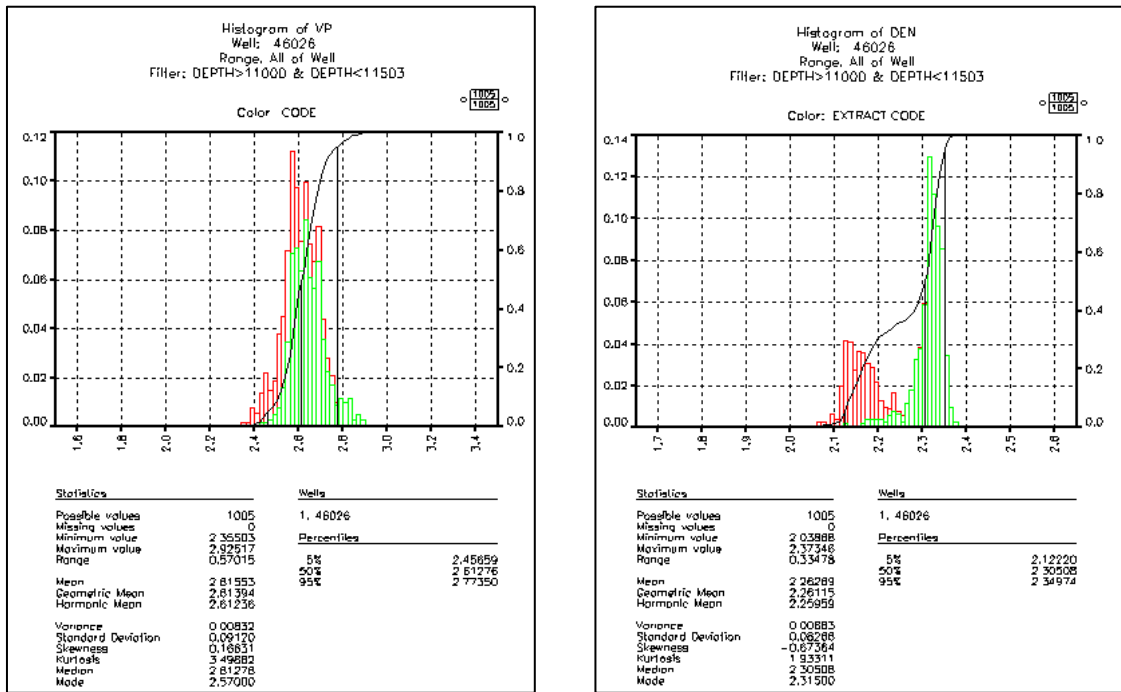


Figure 26. Comparing P-wave velocities (left) and densities (right) of shales (colored green) and wet sands (colored red).

- 3) In some zones, the V_p/V_s ratio is slightly higher in wet sands than in shales.
- 4) Density values for wet sands and shales increase linearly with increasing depth, and shale densities are always greater than sand densities.
- 5) On a V_p vs. V_s cross-plot (Figure 27) logged data were superimposed with different trend lines from literature: mudrock line, Castagna-shales, Castagna-sands (Castagna,

1985), Williams-shale and Williams-sands (Williams, 1990). Logged data appears to have slightly lower V_s for corresponding V_p , comparing with all the trends.

6) Applying the regression on *in situ* data, correlation coefficient of wet sands was 0.85, and shales 0.93. It is interesting to notice that a single trend line for both, wet sands and shales together, showed remarkable correlation coefficient of 0.91.

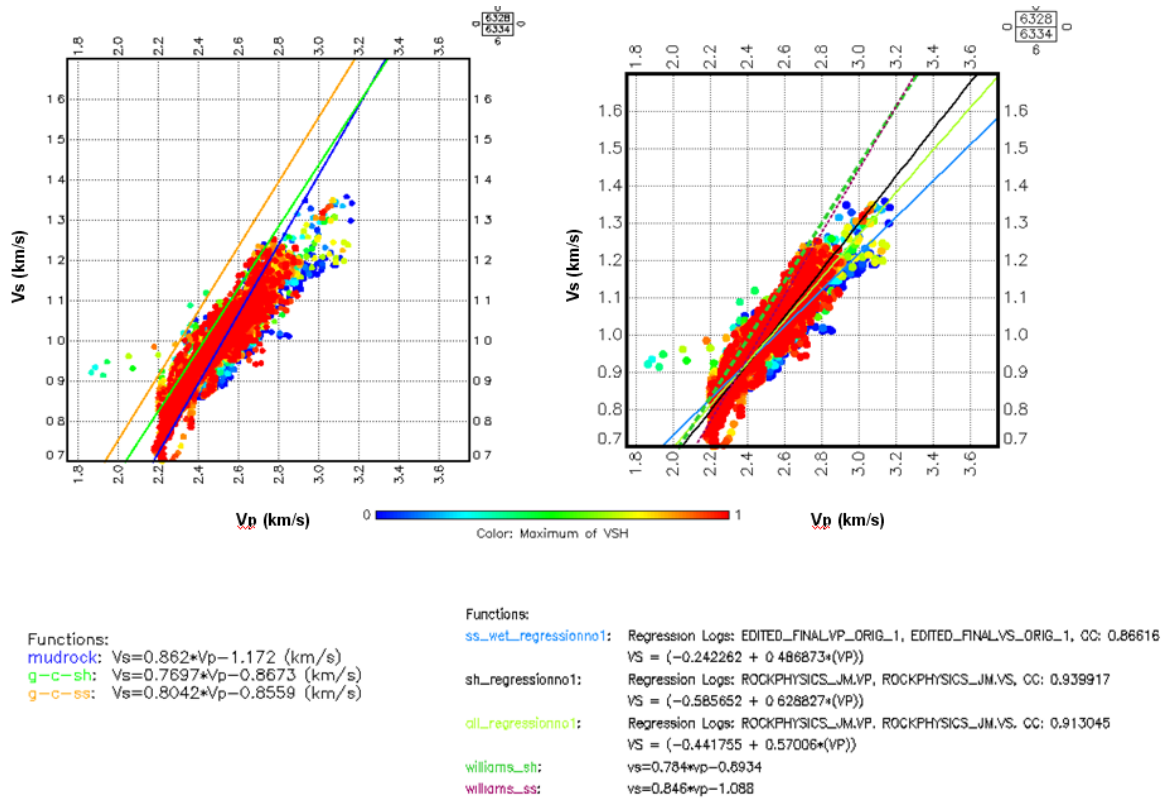


Figure 27. V_p vs. V_s (as logged) with different trend line superimposed. a) Left figure: mudrock line, Castagna-shales, Castagna-sands. b) Right figure: Williams-shale, Williams-sands, regression on *in situ* data for sands, shales and sands-and-shales.

Taking into account all the observations made, our conclusion was that velocities alone (in any of the forms V_p , V_s , V_p/V_s or Poisson' ratio) will not be sufficient tool to distinguish wet sands from shales (Figure 28.a and 28.b).

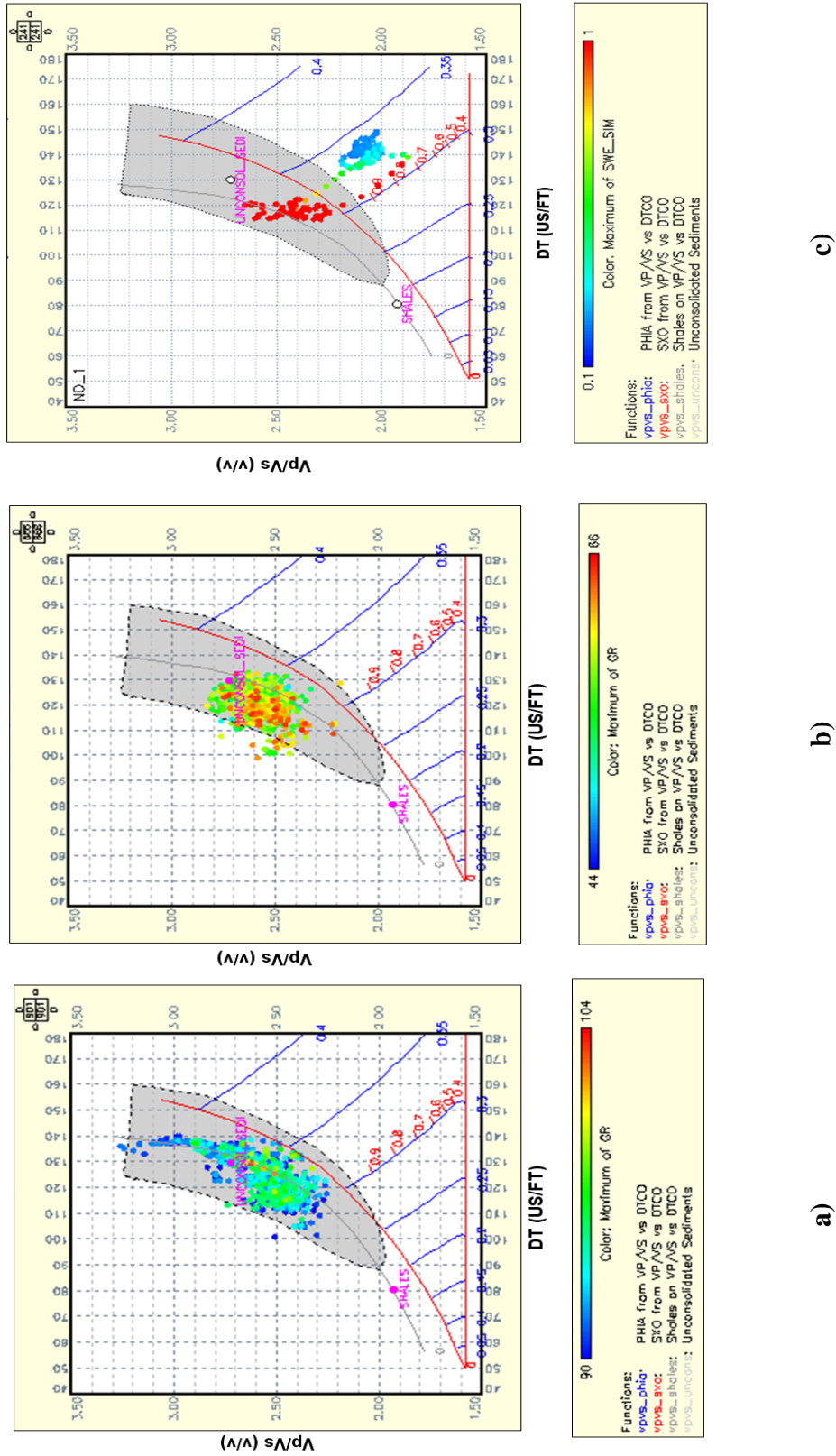


Figure 28. V_p/V_s ratio vs. DTC cross-plot: a) shales, b) wet sands, c) reservoir sands: oil and water (cross-plot idea from Brie *et al.*, 1995).

On the other hand, oil sands differentiate from shales and wet sands from velocity point of view, and contrast is emphasized more when density is included (due to the relatively light oil, and additionally due to very high salinity brine). Figure 28 is a V_p/V_s ratio vs. DTC plot with modeled sand and shale lines (after Brie *et al.*, 1995). The sand model is presented with blue lines representing different porosities, where each of porosity lines has saturation from $S_w=100\%$ to 0% (two red curves). Oil sand (Figure 28.c) plots in a range of porosities 31-33% and saturation plots below the wet sand line. Wet sands from below the reservoir plots above wet sand line, in a zone of “unconsolidated formations” (gray area on the plot). It can be observed that wet sands and shales interfere and overlap in the observed domain.

3.2.1 Petrophysical analysis

Petrophysical analysis included determination of volume of shale, porosity, and water saturation. Volume of shale was estimated from Gamma ray log, using a linear relationship between index of shale and shale volume. Porosity is calculated using density log and corrected for mud invasion (oil-based mud). The Indonesia equation was used for water saturation (Appendix III), with the following parameters: $a=1$, Archie's cementation exponent $m=2$, saturation exponent $n=2$ and resistivity of water at reservoir temperature ($\sim 130^{\circ}\text{F}$) $R_w=0.028$ ohmm (graphically determined through Pickett plot).

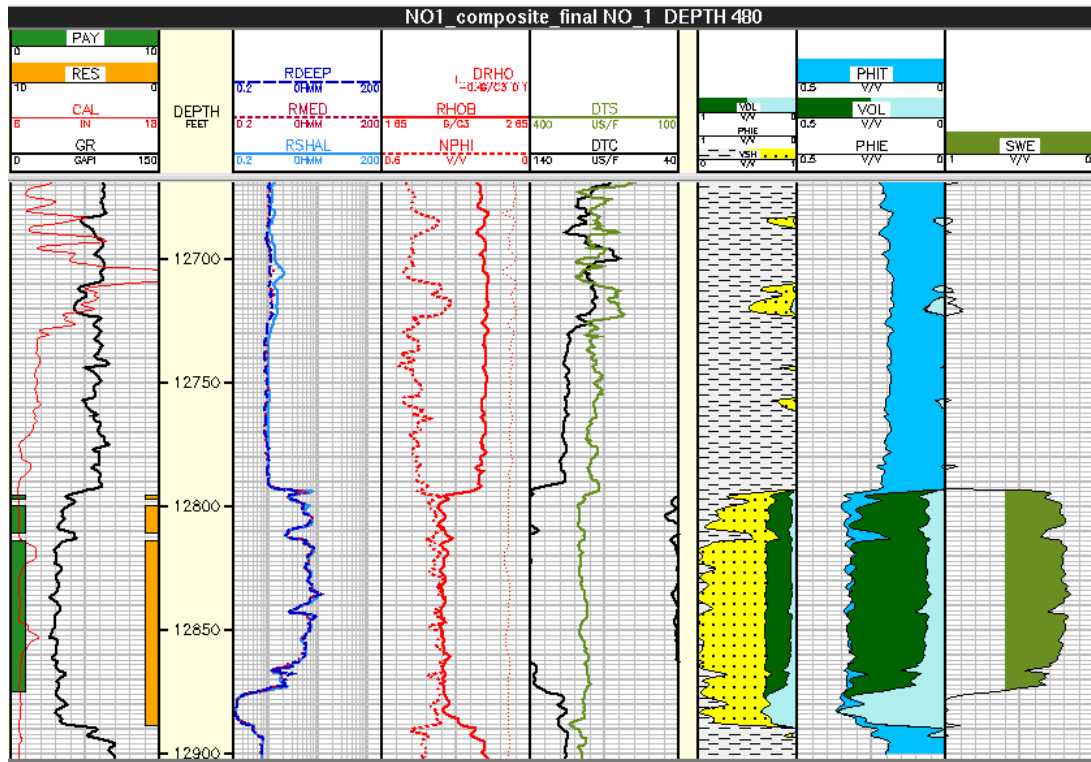


Figure 29. Composite log and petrophysical analysis result for Hoover-1, reservoir zone: 12792-12895 ft (3899-3930 m) MD.

Petrophysical analysis results are presented in Figure 29 in the last three tracks. Track five shows volumes of each component: shale, sand, and fluid. Track six zoom into

the porosities and volume of water in undisturbed formation. In the reservoir zone porosity ranges from 30-34%, and water saturation (track seven) from 15-30% ($S_{oil}=85-70\%$).

The bottom sediments are siliciclastic, and lithologically consist of sands, shaly-sands, and shales. On a density-neutron cross-plot (Figure 30), two zones can be distinguished: sand (color coded by volume of shale as blue, becoming green due to increased amount of shale) and shales (colored as red).

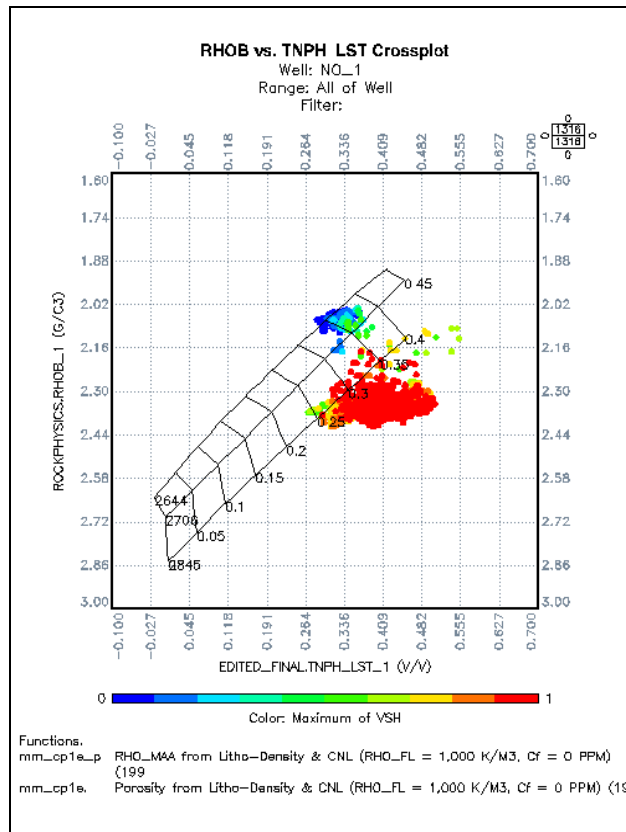


Figure 30. The Neutron-Density cross-plot for interval 12650-12900 ft (3856-3932 m).

The oil-water contact is observed at a depth of 12885 ft (3927 m) measured depth (MD). The reservoir is high permeability, with flow contribution from matrix porosity.

3.2.2 Definition of rock composite (sand-shale system)

The applied model has a solid matrix composed of sands and shales. Pores related to shales are assumed to be filled primarily by bound water (Figure 31). The total pore space is partitioned into clay-related pores and sand-related pores, and only sand-related pores are filled using Gassmann's theory (Figure 32).

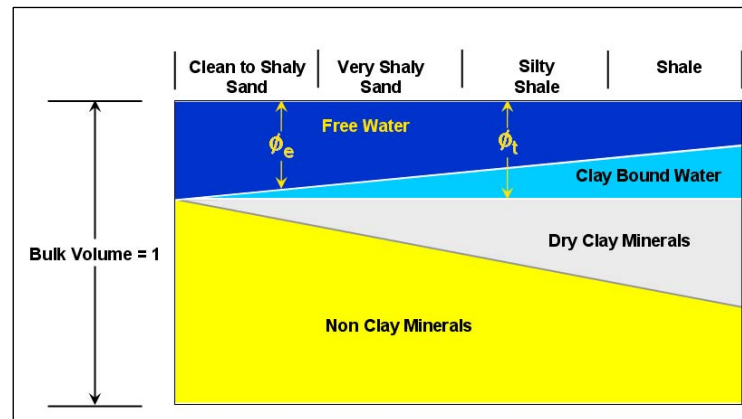


Figure 31. The sand-shale composite (Truman, 1989).

By shales we refer to a fine-grained, sedimentary rock composed mainly of clays (~60%) and other minerals, like quartz, feldspar, *etc.*, characterized by three attributes (Katahara, 2008):

- (1) Clay minerals constitute the load-bearing framework;
- (2) Shales have nanometer pore sizes and nanodarcy permeability;
- (3) Surface area is large, and water is adsorbed on surfaces or bound inside clay platelets.

As seen from the above attributes, shale definition encompasses both grain size (<3.9 micrometers), and mineralogy (denoting illite, smectite, chlorite, kaolinite, and other hydrous phyllosilicates). These two meanings of clay overlap significantly in practice but are not identical.

The effect of clay on seismic properties depends on the amount (volume fraction) of clay, position of the clay particle in the rock matrix (laminated, structural, dispersed), and on the clay type (Steiber *et al.*, 1775). Minear (1982) showed that laminated and structural clay have similar effects on moduli, which are dominant comparing with the effect of dispersed clay. On the contrary, Stanford models focus on dispersed clay effect on elastic properties (Marion, 1990; *etc.*). Han (1986) observed that velocities correlate to clay content only, and not to be sensitive to their location. For our modeling, we assume shale is part of the solid matrix.

3.2.3 Inverting for rock frame properties using Gassmann fluid substitution

To invert properties for dry rock moduli, the Gassmann equation is used through the following procedure (modified after Smith *et al.*, 2003):

1. Log edits and interpretation.
2. S-wave velocity estimation (if necessary). S-wave velocity (DTS) has been logged in Well No-1 in Hoover field.
3. Calculate bulk and shear moduli for *in situ* conditions using the following equation:

$$K_{sat} = \rho_b \left(V_p^2 - \frac{4}{3} V_s^2 \right) \quad (20)$$

$$\mu_{sat} = \rho_b V_s^2, \quad (21)$$

where ρ_b , V_p , V_s are density and velocities (sonic travel time) as logged, without any correction applied.

4. Calculate K_0 based on lithology estimates (volume of shale). Hoover lithology is siliciclastic sands, shales, and mixture of the two. So, we assume that the formation is comprised of quartz minerals and shales, that it is homogeneous and isotropic in macro sense.

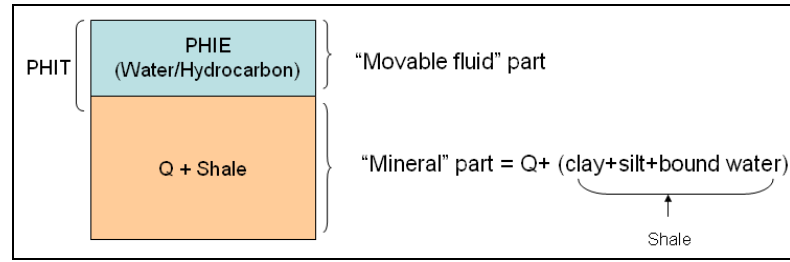


Figure 32. The sand-shale system, as modeled (Q=quartz).

We assume that shales above, below, and within the reservoir are the same, and that the difference between total and effective porosity is due to clay-bounded water.

We assume the bulk modulus for quartz is 37 GPa, and the shear modulus for quartz is 38 GPa. Shale properties have been extracted from the logs in a zone with the highest shale fraction (volume of shale equal to 100%). Bulk modulus for shales is 14 GPa, shear modulus for shales is 2.7 GPa. Then we mixed quartz and shales using the Hill average (Mavko *et al.*, 1998):

$$K_{Reuss} = \left(\frac{f_1}{K_1} + \frac{f_2}{K_2} \right)^{-1} \quad (22)$$

$$K_{Vight} = (f_1 K_1 + f_2 K_2) \quad (23)$$

$$K_{vrh} = \frac{1}{2} (K_{Voigt} + K_{Reuss}) \quad (24)$$

where,

f_1 and f_2 = volume fractions of sands and shales;

K_1 and K_2 = quartz and shale bulk moduli.

Mineral modulus for the mixture is given in the Figure 33.

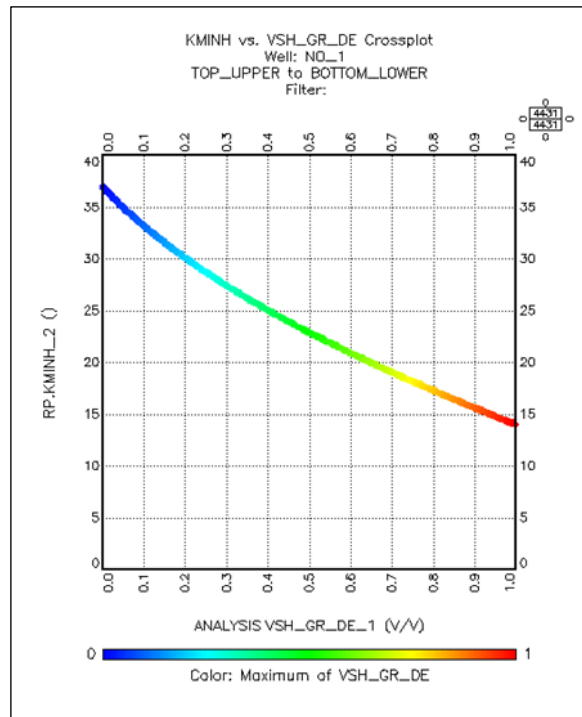


Figure 33. Mixing moduli using the Hill average (color-coded by volume of shale).

5. Calculate fluid properties. Fluid properties estimation has been described in the previous section. The same properties have been used here.
6. Mix fluid densities and moduli for *in situ* case according to S_w .
7. Calculate K_{dry} . “The ‘dry’ frame modulus refers to the incremental bulk deformation resulting from an increment of applied confining pressure with pore

pressure held constant” (Mavko *et al.*, 1998). It is a function of porosity, mineral modulus, fluid modulus and modulus of a saturated rock, and is given by:

$$K_{dry} = \frac{K_{sat} \left(\frac{\phi K_0}{K_{fl}} + 1 - \phi \right) - K_0}{\frac{\phi K_0}{K_{fl}} + \frac{K_{sat}}{K_0} - 1 - \phi} \quad (25)$$

8. Calculate the “dry” bulk density (density of fluid equal to zero).
9. Calculate the “dry” compressional and shear velocity.

3.3 Results and discussion

The derived K_{dry} curve is presented in the sixth track in Figure 34 (green curve). It reaches 14 GPa in shale zones, which is the extracted value for moduli from logged data in a shaliest interval in the section. In the sand zone it ranges from 2.5-4.5 GPa. It seems that shale content reduces the moduli in sandstone, hence, decreasing velocities.

Our model assumes that a dry rock behaves as a porous linear elastic solid. When the rock is compressed, the frame elastically compresses; the compression squeezes the pore fluid, which induces an increase of pore pressure. This pore pressure resists the compression of the pore space, hence, stiffening the rock.

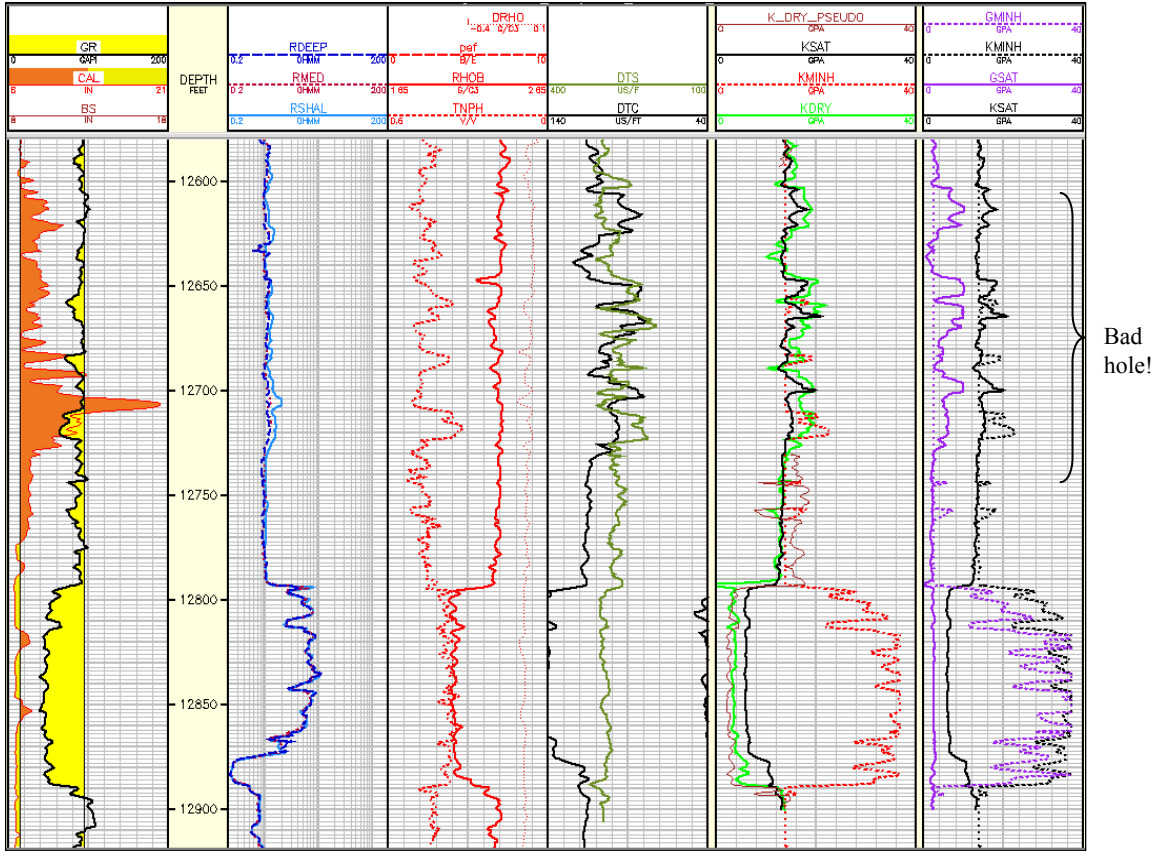


Figure 34. Estimated “dry” bulk modulus, KDRY, presented as green curve in track five. KSAT is bulk modulus at initial saturation (black curve in track five), and Hill average for mineral bulk modulus, KMINH (red curve in track five).

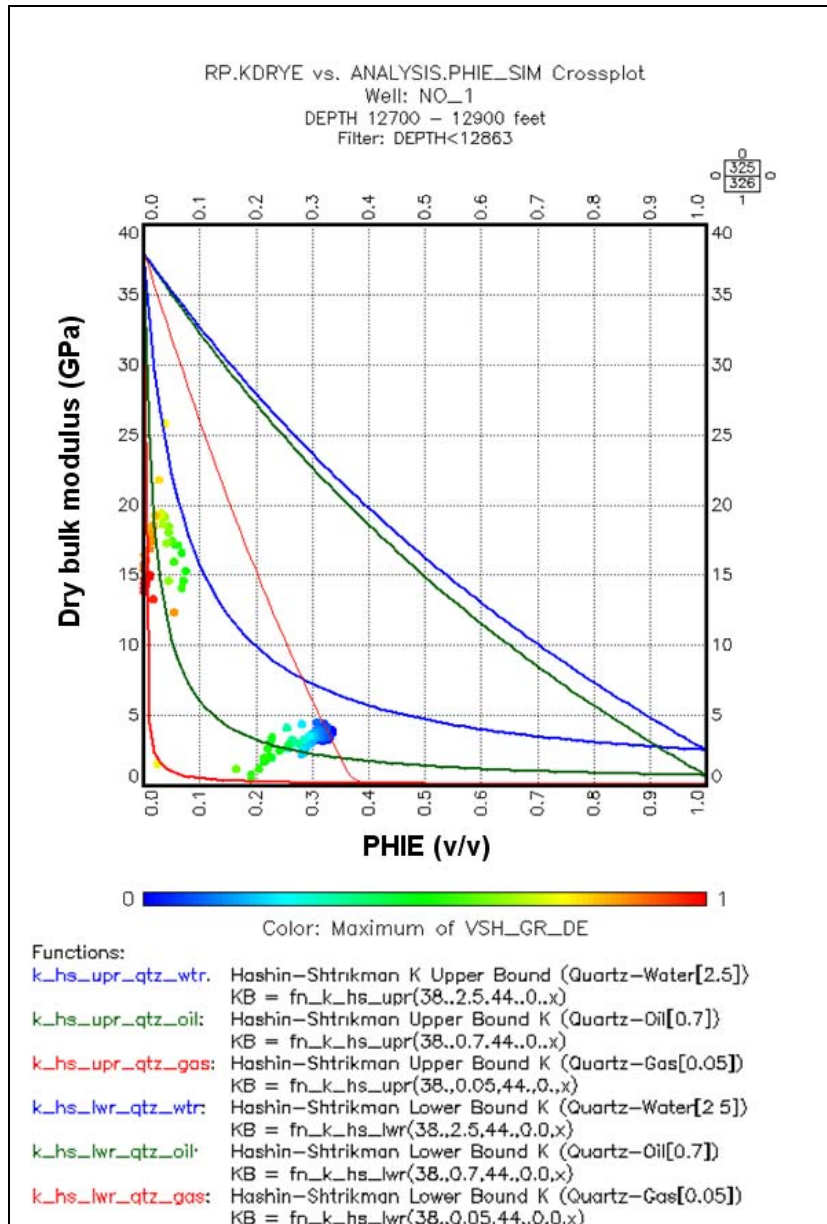


Figure 35. “Dry” bulk modulus determined from logs superimposed with Hashin-Shtrikman upper and lower bounds for rocks saturated with different fluids: water (blue curve), oil (green curve), and gas (red curve), at surface condition. Steep red curve from Murphy (1993).

One can see the effects of porosity and clay content on K_{dry} (Figure 35). The regression equation has been developed for K_{dry} as a function of effective porosity (Φ_{eff})

and volume of shale (V_{sh}), for a relatively small interval around the reservoir. It has the following form:

$$K_{dry} = 29.5 - 78.3\phi_{eff} - 15.5V_{sh} \quad , \quad (26)$$

where Φ_{eff} , and V_{sh} are in p.u. and K_{dry} in GPa.

Regression of K_{dry} versus porosity and clay volume provided the quartz point ($K_{dry}=29.5$ GPa at zero porosity), the clay point ($K_{dry}=14$ GPa), as well as the dependence on porosity. When reduced to clean sand (volume of shale equal to zero), it shows relatively good fit with Murphy trend line (Figure 36) in the range of porosities 25-35%.

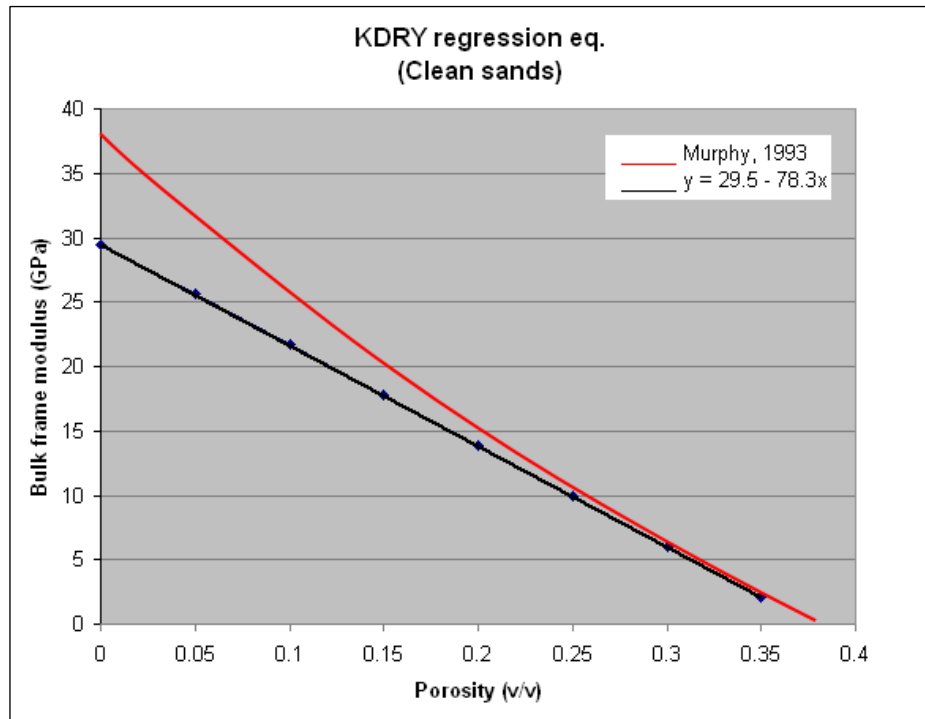


Figure 36. Comparison between derived regression equation and Murphy curve (Murphy, 1993) for clean sands, in bulk modulus vs. porosity plane.

From all the parameters in Gassmann equation, K_{dry} is probably the most difficult to estimate. It will usually accumulate errors that were propagated through all the computations. Listed are some of the sources for anomalous K_{dry} values:

- 1) Matrix properties are incorrect;
- 2) Fluid properties are incorrect;
- 3) Initial assessments of porosities and/or water saturation are incorrect;
- 4) Velocities incorrect;
- 5) Shale/clay can cause the problems for a variety of reasons when considering the Gassmann assumptions. The elastic moduli of clay are much smaller than those of quartz, feldspar, calcite, and dolomite. Thus, large amounts of clay can cause the average mineral method to introduce errors. Elastic properties of clay minerals are not well known although some clay properties measurements have been published (Wang *et al.*, 2001), and are often widely different. Furthermore, the textural distribution of clay minerals (*e.g.* pore filling clay and structural clay) has a significant effect on the elastic properties, (Minear, 1982). Katahara (2004) suggests an approach to modeling laminated shaly-sands that relies on empirical trends. Additionally, properties determined by laboratory ultrasonic measurements differ from those properties measured in the field, *etc.*

One of the recommended techniques for evaluating dry properties is to compute the ratio of K_{dry} to G_{dry} (Smith *et al.*, 2003). For clean sands, this ratio is usually close to 1 (Wang, 2001), whereas for shaley sands it may approach 2–3.

3.4 Rock frame models comparison

In previous chapters several models were described: effective medium model, heuristic models (Krief and CPM), and Gassmann equation inverted for “dry” properties from real data at Hoover field. Finally, we would like to compare and contrast them focusing on rock frame modulus: K_{dry} .

Figure 37 illustrates relatively good fit between K_{dry} derived from logged data superimposed with theoretically predicted curve (Hertz-Mindlin and Hashin-Shtrikman theory).

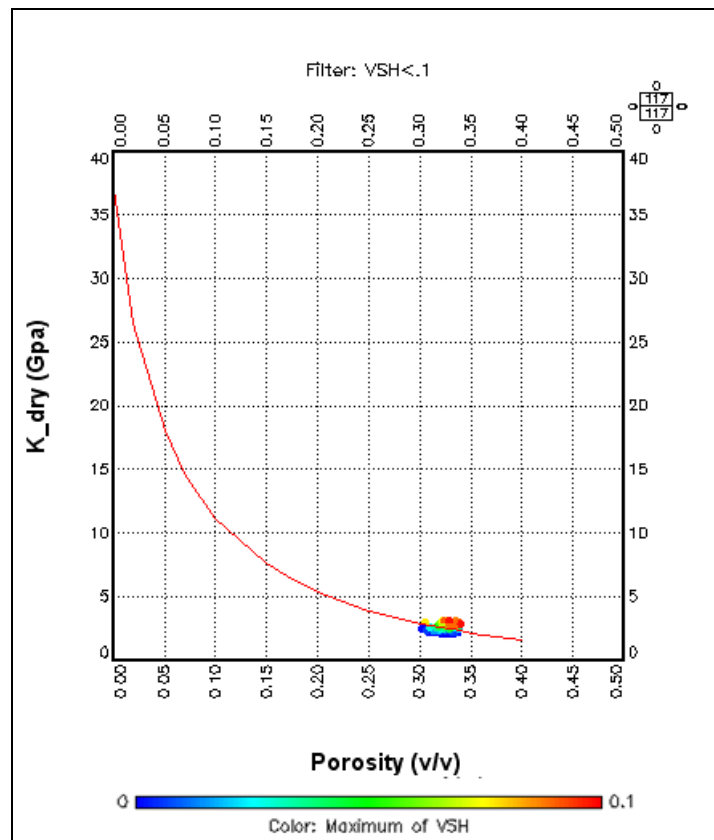


Figure 37. Log-derived dry bulk modulus superimposed with theoretically predicted curve.

Krief and CPM, applied on real data, show the overprediction of K_{dry} : K_{dry_KRIEF} being in a range of 5.0-7.5 GPa, K_{dry_CPM} 6.0-8.0 GPa, which is reaching the bulk modulus value for saturated rock, and being almost twice higher than the K_{dry} derived from logged data (Figure 38). Thus, it was considered as inappropriate for modeling unconsolidated formations.

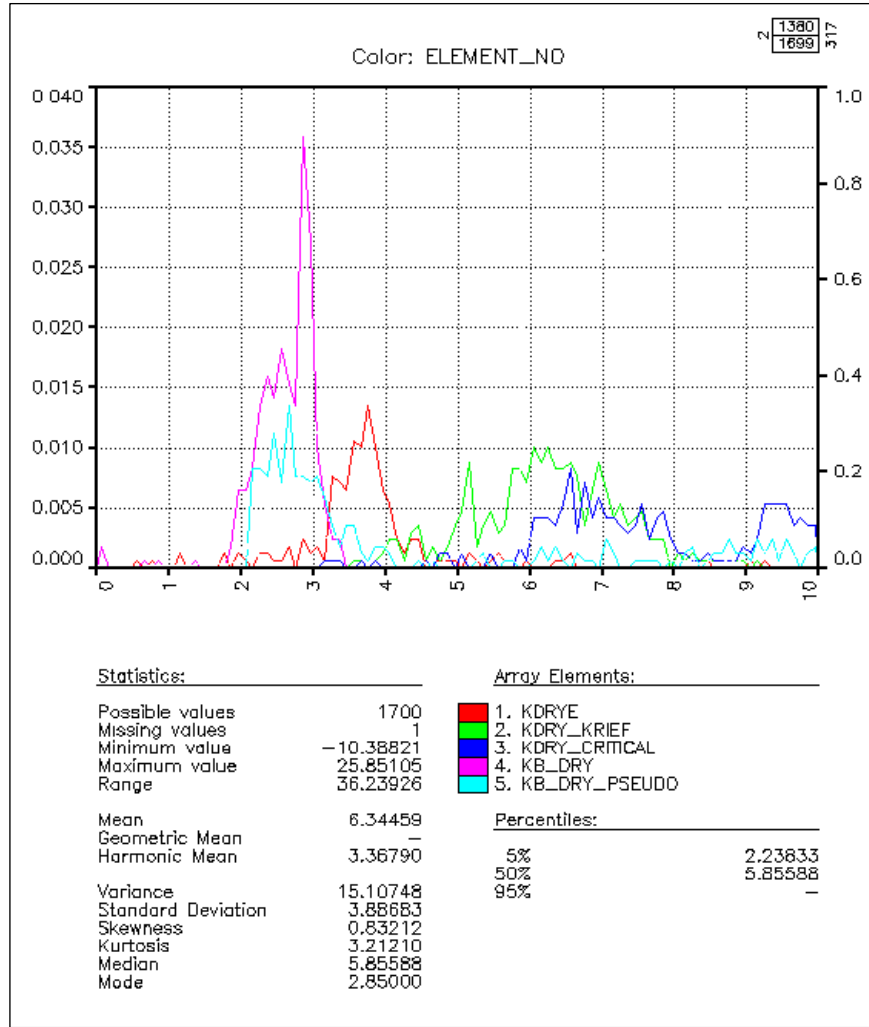


Figure 38. “Dry” modulus vs. porosity plane. Comparison between K_{dry} s for: K_{dry} derived from Hoover logged data with effective porosity (KDRYE), effective porosity KDRYE constrained with K_{dry} -to- μ_{dry} ratio (KB_dry_PSEUDO; Smith *et al.*, 2003), K_{dry} from Krief (K_{dry_KRIEF}), CPM ($K_{dry_Critical}$), K_{dry} derived from logged data with total porosity (KB_dry).

4. CROSS-PLOT ANALYSIS: Rock physics templates

Rock physics templates (RPT) are charts of rock physics models used for prediction of lithology and hydrocarbons from well log and seismic data (Odegaard *et al.*, 2004). The general idea for building a template is to combine depositional and diagenetic trends, usually using velocity-porosity relations, with Gassmann fluid substitution (Avseth *et al.*, 2001), so that both rock/lithology and fluid effects are encountered.

The starting assumption is that if a match between a theoretically predicted value and measured data is achieved, then the theoretical model can be considered as appropriate. In that sense, building a rock physics frame for quantitative seismic analysis can be viewed as a way to constrain theoretical rock physics models to local geologic parameters, including lithology (mineral composition and texture), burial depth, pressure, and temperature.

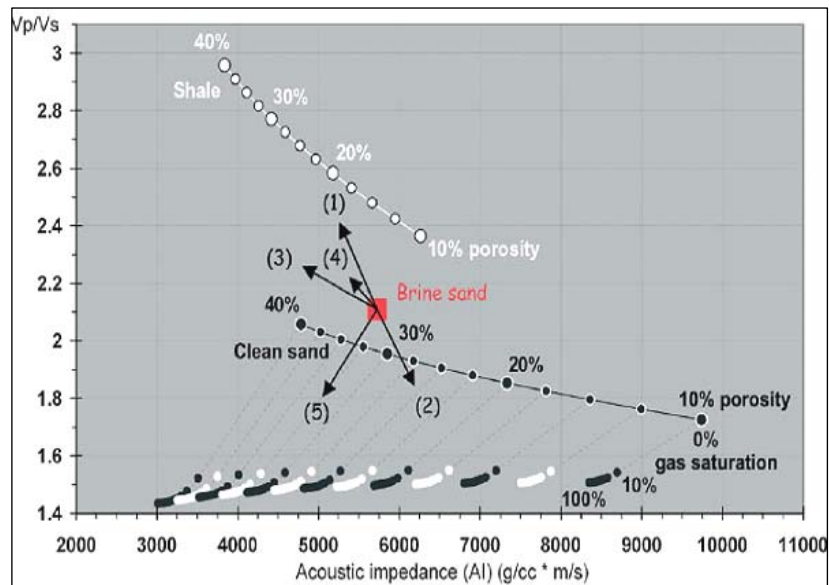


Figure 39. Rock physics template in V_p/V_s vs. AI (Odegaard *et al.*, 2004).

Figure 39 includes a background shale-trend line, a brine-sand-trend line, and curves for increasing gas saturation as a function of porosity on a rock physics template in V_p/V_s vs. AI cross-plot domain. The black arrows shows (conceptually) the effects of various geologic trends: 1) increasing shaliness, 2) increasing cement volume, 3) increasing porosity, 4) decreasing effective pressure, 5) increasing gas saturation. The ambiguity of interpretation is noticeable. For example, increase in shale content can be misinterpreted with decreasing in effective pressure, *etc.*

The initial step in creating a template is determining the appropriate rock physics model. Theoretical rock physics models are calibrated and validated to local geology and well log data (primarily sonic and density log, and any combination of the two). Well log data are analyzed to define the reservoir and surrounding shale (gamma ray, resistivity, sonic, density, and neutron log). Then the rock is diagnosed by superimposing theoretical rock physics curves on the V_p vs. porosity/density-porosity plot, modulus vs. porosity plot, *etc.* When analyzing well logs to derive velocity-porosity trend, it is important to map the data to a common fluid. Otherwise, the effect of pore fluid and rock frame become mixed.

Model behavior is investigated through cross-plotting different properties: V_p vs. RHOB, V_p vs. V_s , V_p/V_s vs. DTC, AI vs. SI, V_p/V_s vs. AI, *etc.* Because of the convenience and agreement with seismic inversion results, preferred plots usually are V_p/V_s vs. AI, or simply AI vs. SI.

4.1 Methodology and Algorithm

The following steps are used to build a template for the Hoover field (Figure 40):

1. Estimate dry bulk and shear moduli at initial porosity, applying Hertz-Mindlin theory.
2. Select zero porosity mineral point ($\Phi=0$; K and μ of the solid material);
3. Interpolate between the two-end members using modified Hashin-Shtrikman modeling. If at high porosities velocity values are close to those obtained by combining Hashin-Shtrikman and Hertz-Mindlin theory, then there is no contact cement and the rock is held together by confining pressure only (Dvorkin et al, 1996).
4. Perform Gassmann fluid substitution to calculate moduli at different saturations and different porosities. From calculated moduli and density at new saturation, determine V_p and V_s .
5. Match the data to verify model accuracy.
6. Analyze different cross-plots to emphasize fluid and lithology component: V_p/V_s vs. AI, AI vs. SI, λ vs. μ , *etc.*

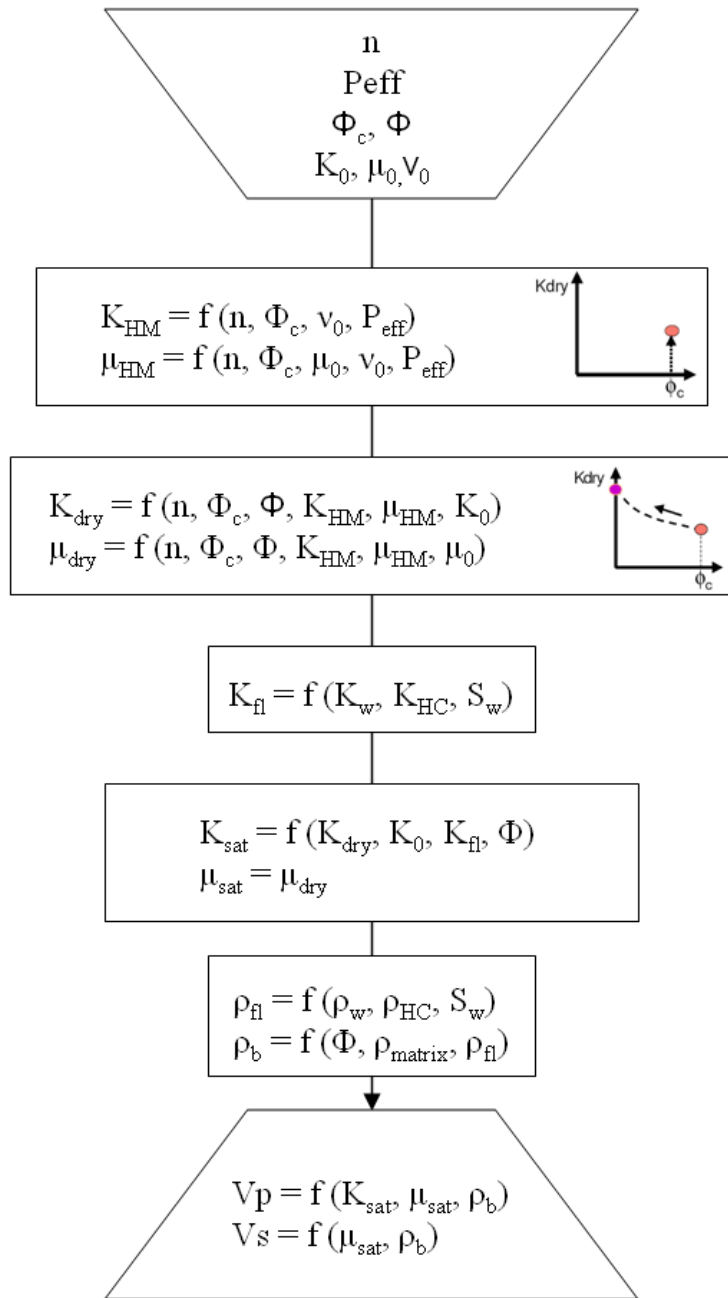


Figure 40. Rock physics template algorithm.

4.2 Final plot and application

The resulting rock physics model for sands and shales, with log data superimposed, is presented in a V_p/V_s vs. AI cross-plot, color coded by DTC (Figure 41) and DTS (Fig 42). By different coloring the data, the fluid vs. lithology effect is noticeable: DTS mainly reflects lithology component and DTC reflecting both fluid and lithology.

Two trend lines present shale and sand line. Modeled shale porosity range from 20-60%, and modeled sand porosity 0-30%. Each of porosity sand lines has its saturation line, which starts as 100% brine saturated sand, and end as oil-saturated.

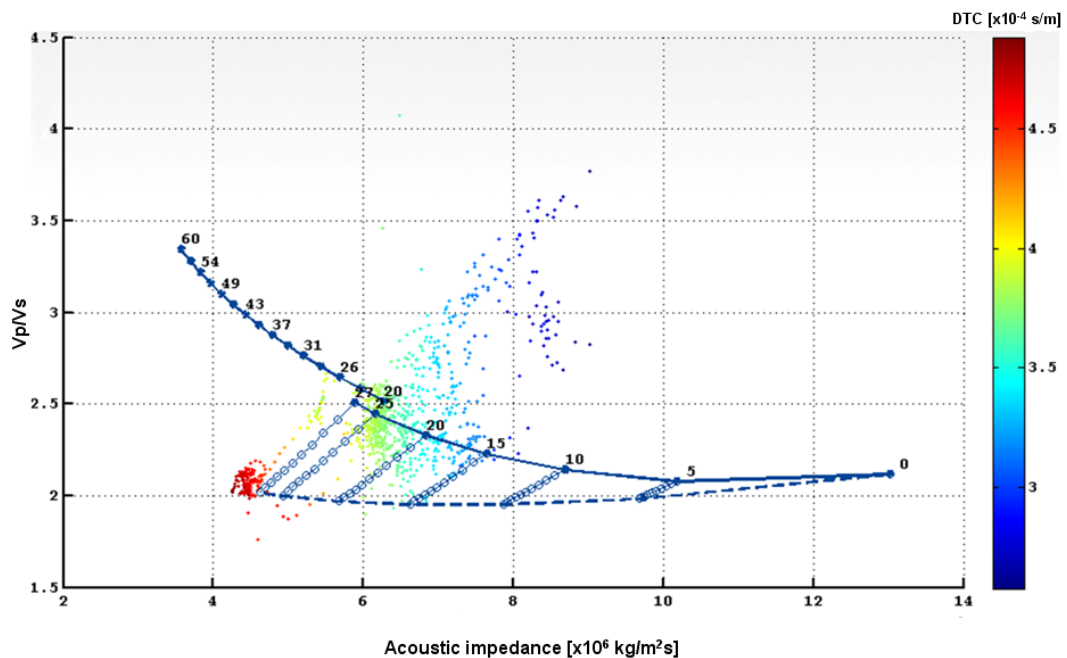


Figure 41. Rock physics template in V_p/V_s vs. AI domain for Hoover reservoir (oil sand, wet sand below oil-water contact, shales around the reservoir. Depth 12780-12900 ft (3896-3932 m). Each of porosity sand lines has its saturation line, which starts as 100% brine-saturated sand, and end as oil-saturated.

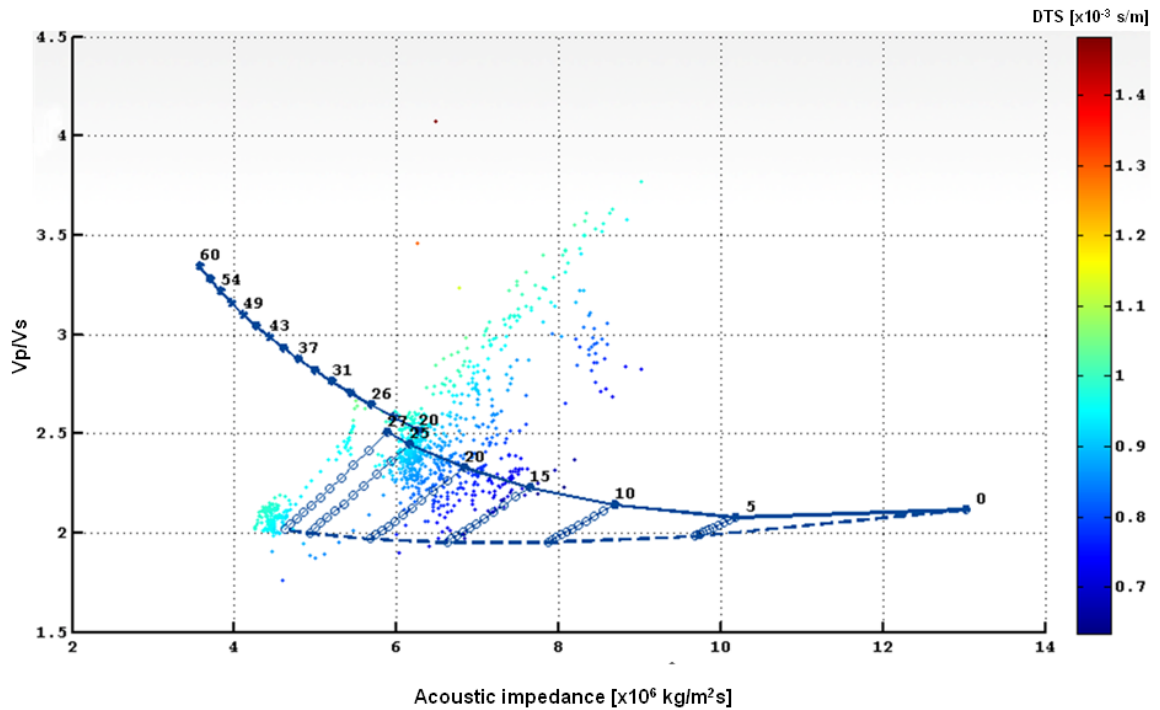


Figure 42. Rock physics template in V_p/V_s vs. AI for Hoover reservoir (oil sand, wet sand below oil-water contact, shales around the reservoir. Depth 12780-12900 ft (3896-3932 m).

Some applications of a rock physics template (RPT) as an interpretation tool are provided below. It can be used for quality control of well log data, which can be observed on Figure 41 and Figure 42. The cloud of dots in the middle of the figure presents bad data preserved with the purpose to test the RPT.

It allows well log analysis primarily in a qualitative and partially in a quantitative sense (clay content, cement volume, degree of sorting). It gives a rough estimate of porosity (a few % error, which is not accurate enough for petrophysical analysis), and less reliable results for saturation.

From a seismic interpretation point of view, the template allows the assessment of seismic detectability of lithologies (seismic lithofacies - defined by clay content, grain size, bedding configuration, and fluids. However, they must be used with care. These are general conclusions, and the applicability of the methodology will strongly depend on geological setting and types of rock and fluids present. Note that RPT is almost always basin-specific, *e.g.* locally geologically constrained.

The rock physics templates used in diagnosing the rocks suffer from two important issues: ambiguity in the velocity-porosity plane (for examples ambiguity between clay content and sorting when modeling sands), and the issue of resolution (rock physics models usually assume homogeneous rock, which is usually not the case for *in situ* conditions, whether it is seen through core scale, logging tools, or seismic).

4.3 Probabilistic modeling

The methodology discussed in previous sections is a deterministic approach. As most of the input parameters include uncertainty due to our limited knowledge, it is usually hard to exactly describe the existing state or future outcome with a single value. Thus, our modeling has been extended to incorporate uncertainties, resulting in prediction of a range of expected values, instead of a single one.

From a modeling perspective, the same procedure has been followed for creating a rock physics template. Instead of having a single input value, the initial system this time was defined through a range of expected values (Figure 43).

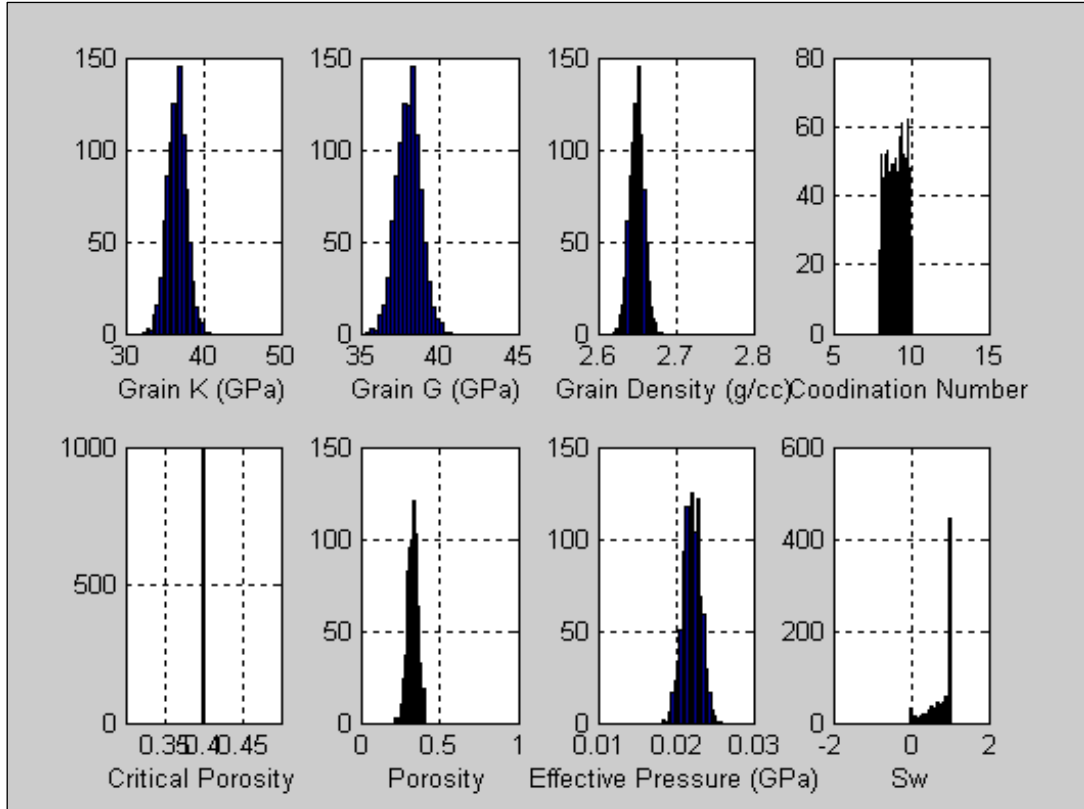


Figure 43. Input parameters distribution.

Three types of distributions were used: (1) Gaussian for grain/mineral bulk modulus, grain shear modulus, grain density, porosity, effective pressure, and saturation; (2) constant for coordination number; and (3) single value for critical porosity.

The output results are given through a range of values presented in Figures 44-46, for dry properties and oil- and water-saturated.

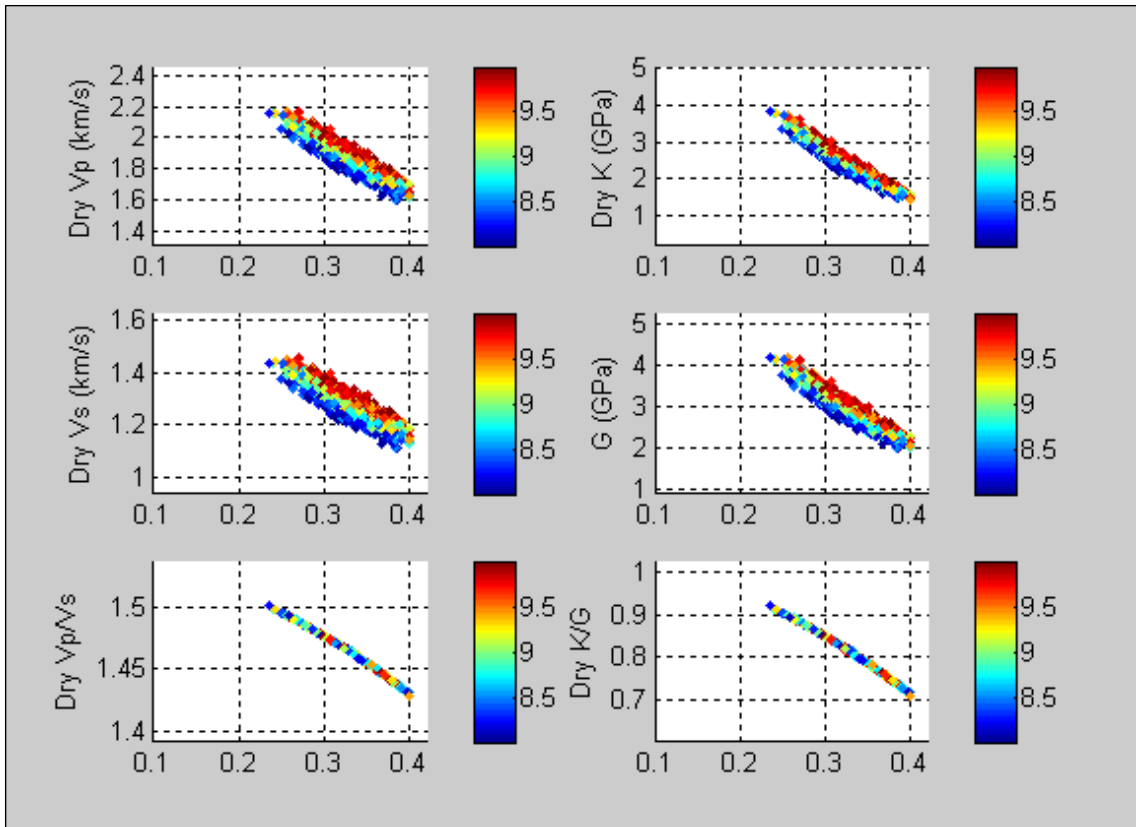


Figure 44. Rock frame properties (color coded by coordination number). X-axis: porosity, y-axis: dry rock properties (P-wave and S-wave velocities, V_p - V_s ratio, Bulk modulus, Shear modulus, Bulk-shear modulus ratio). Note that dry V_p/V_s are independent of coordination number.

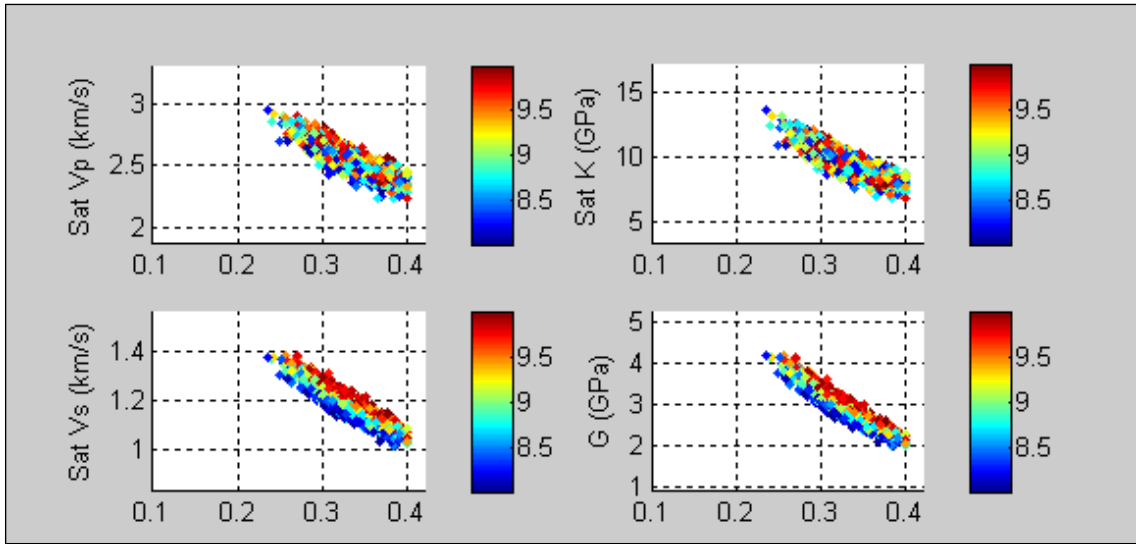


Figure 45. Rock properties for range of saturations, from $S_{oil}=1$ to $S_w=1$ (color coded by coordination number). X-axis: porosity, y-axis: saturated rock properties (P-wave and S-wave velocities, Bulk modulus, and Shear modulus).

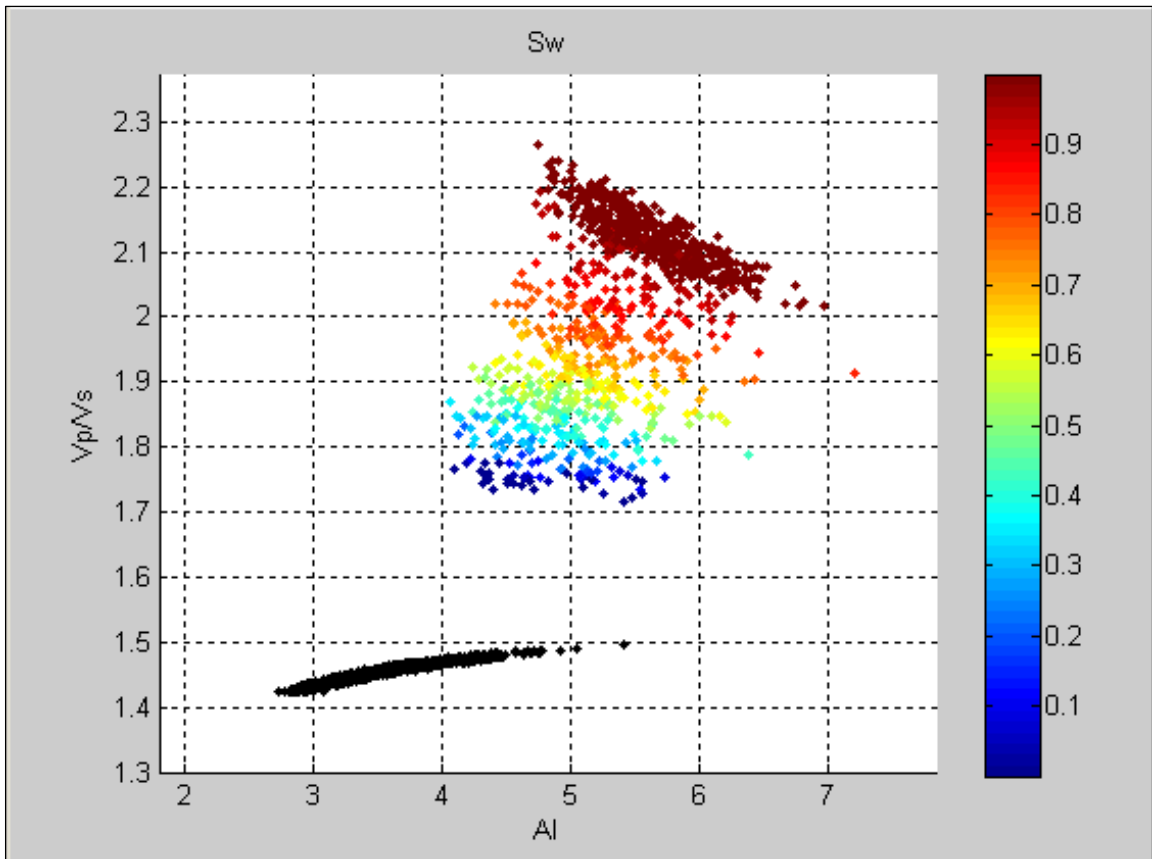


Figure 46. Final plot V_p - V_s vs AI cross-plot. Color coded by water saturation: red=100% brine; blue=100% oil. The black dots on the plot represent the dry rock.

5. CONCLUSION

A model has been built for an unconsolidated GOM reservoir, respecting the assumption that if well log data points fall close to a theoretical line in velocity-porosity or modulus-porosity plane, then the internal structure of a rock is similar to the idealized structure predicted by theoretical model. The criteria for the accuracy were primarily the fit to the logged data, and in part comparison to the similar rocks from the literature.

Several models have been compared: linear forms: the Critical porosity model (CPM), the Murphy data relationship (Murphy, 1993), and the derived equation for Hoover field from logged data; and non-linear forms: the Krief model and an effective medium model (Herz-Mindlin combined with Hashin-Shtrikman theory). Some conclusions have been made:

- In general, a non-linear fit better represents the velocity-porosity (modulus-porosity) behavior.
- The CPM and Krief model are too stiff and resulting velocities are overpredicted. The Krief model is closer to the measured data, but still not soft enough. Changing the exponent might result in achieving a better fit.
- Hertz-Mindlin theory accurately predicts the bulk modulus and overpredicts shear modulus due to the non-slip assumption. Applying the correction ($\mu_{HM}/\mu_{logged}=1.3$ in the Hoover field particular case) results in fitting the logged data and reconstructing accurate velocities.
- Hertz-Mindlin theory incorporates the effective pressure effect on the elastic properties of rock frame. Thus, it can be used to monitor/model changes in elastic

properties due to change in pressures during production of an oil/gas field. Additionally, combined with Gassmann's fluid substitution, it will model saturation changes as well, assuming uniform saturation (which might not be the case). If changes are remarkable enough, they can be monitored using 4D seismic.

- From log data, a linear equation is developed that relates porosities, clay content, and dry modulus. It fits the Murphy curve in clean high porosity sands. According to Vernik, 1998, porosity and clay are not the main controlling parameters for velocity prediction in these rocks. He claims that they are less important compared with grain sorting, loading history, and initial cementation, which makes unconsolidated rocks non-unique. Our data could not lead us to that conclusion.
- Shear velocities vary linearly with compressional velocities for wet sand and shale. The linear relationship found in this study is consistent with V_p - V_s relationships found in other studies, although the coefficients are somewhat different and require local calibration. A single trend line has been selected to best represent both, wet sands and shales.
- The magnitude of the fluid effect is largely increased in unconsolidated rocks compared with any other rock. It is possible to distinguish oil sands from both wet sands and shales in different cross-plot domains, due to the high porosity rock frame and difference in fluid properties (light oil vs. high salinity brine). It suggests the use of rock physics templates in analysis of seismic inversion results. The applied methodology can be expanded to describe lithofacies and depositional environments from seismic data in deep-water clastic depositional systems. Due to ambiguities, it has to be used with great care.

REFERENCES

- Avseth, P., 2000, Combining rock physics and sedimentology for seismic reservoir characterization of North Sea turbidite systems: Ph.D. dissertation, Stanford University.
- Avseth, P., Flesche, H., and van Wijngaarden, A-J., 2003, AVO classification of lithology and pore fluids constrained by rock physics depth trends: *The Leading Edge*, **22**, p. 1004-1011.
- Avseth, P., and Bachrach, R., 2005, Seismic properties of unconsolidated sands: Tangential stiffness, V_p/V_s ratios and diagenesis: 75th Annual Meeting, SEG, Expanded Abstracts, p. 1473-1476.
- Avseth, P., Mukerji, T., and Mavko, G., 2005, Quantitative seismic interpretation – Applying rock physics tools to reduce interpretation risk, Cambridge University Press.
- Avseth, P., Wijngaarden, A.J., Mavko, G., and Johansen, T. A., 2006, Combined porosity, saturation and net-to-gross estimation from rock physics templates: 76th Annual Meeting, SEG, Expanded Abstracts, p. 1856-1860.
- Bachrach, R., Dvorkin J., and Nur, A. M., 2000, Seismic velocities and Poisson's ratio of shallow unconsolidated sands: *Geophysics*, **65**, p. 559-564.
- Batzle, M., and Wang, Z., 1992, Seismic properties of pore fluids: *Geophysics*, **57**, p. 1396–1408.
- Berryman, J. G., 1999, Tutorial: Origin of Gassmann's equations, *Geophysics*, **64**, p. 1627-1629.
- Beryman, J. G., and Milton, G. W., 1991, Exact results for generalized Gassmann's equations in composite porous media with two constituents: *Geophysics*, **56**, No. 12, p. 1950-1960.
- Blangy, J. P., Strandenest, D., Moos, D., and Nur, A., 1992, Ultrasonic velocities in sands-revisited: *Geophysics*, **58**, p. 344-356.
- Brie, A., Pampuri, F., Marsala, A. F., and Meazza, O., 1995, Shear sonic interpretation in gas-bearing sands: SPE paper 30595, p. 701-710.
- Burtz, O., and Matteucci, G., 2002, Model-based calibration of band-limited impedance data: Hoover field: 72nd Annual Mtg, SEG, Expanded abstract.

- Castagna, J. P., Batzle, M. L., and Eastwood, R. L., 1985, Relationships between compressional-wave and shear-wave velocities in clastic silicate rocks: *Geophysics*, **50**, p. 571–581.
- Castagna, J. P., Batzle, M. L., and Kan, T. K., 1993, Rock physics—the link between rock properties and AVO response, *in* Castagna, J. P. and Backus, M. M., Eds., *Offset-dependent reflectivity—theory and practice of AVO analysis*, SEG, p. 131–171.
- Chen, W., 1995, AVO in azimuthally anisotropic media: Unpublished Ph.D. thesis, Stanford University.
- Deng, Ji – Xin, Han, D., and Liu, J., 2006: The effects of geologic parameter variation on the A-B Cross-plot of sand reservoir, Fluid/DHI Annual Mtg.
- Digby, P. J., 1981, The effective elastic moduli of porous granular rocks: *J. Appl. Mech.*, **48**, p. 803-808.
- Dvorkin, J., and Gutierrez, M., 2001, Textural sorting effect on elastic velocities: 71st Annual Meeting, SEG, Expanded Abstracts.
- Dvorkin, J., and Nur, A., 1996: Elasticity of high-porosity sandstones, Theory for two North Sea data sets, *Geophysics*, **61**, p. 559-564.
- Faust, L. Y., 1951, Seismic velocity as a function of depth and geologic time: *Geophysics*, **16**, p. 192–206.
- Gardner, G., Gardner, L., and Gregory, A., 1974 Formation velocity and density – the diagnostic basis for stratigraphic traps: *Geophysics*, **39**, p. 770-780.
- Gassmann, F., 1951, Uber die elastizitat poroser medien: *Vier. der Natur Gesellschaft*, **96**, p. 1-23.
- Greenberg, M. L., and Castagna, J. P., 1992, Shear-wave velocity estimation in porous rocks; theoretical formulation, preliminary verification and applications: *Geophysical Prospecting*, **40**, p. 195-209.
- Han, D., 1986, Effects of porosity and clay content on acoustic properties of sandstones and unconsolidated sediments: Ph. D. dissertation, Stanford University.
- Han, D.H., Nur, A., and Morgan, D., 1986, Effects of porosity and clay content on wave velocities in sandstones: *Geophysics*, **51**, p. 2093-2107.
- Han, D., 2003, Velocities and porosity of deepwater reservoir sands: Expanded abstract, Fluid/DHI Annual Meeting.

- Jizba, D., 1991, Mechanical and acoustic properties of sandstones and shales: Unpublished Ph.D thesis, Stanford University.
- Johnstad, S. E., Dvorkin, J., 1999, Velocity-porosity trends in well log data, SEG Expanded abstracts.
- Krief, M., Garat, J., Stellingwerff, J., and Ventre, J., 1990, A petrophysical interpretation using the velocities of P and S waves (full-waveform sonic): *The Log Analyst*, **31**, p. 355-369.
- Katahara, K., 2008, What is shale to a petrophysicist: *The Leading Edge*, **27**, p. 738-741.
- Kuster, G.T. and Toksöz, M.N., 1974, Velocity and attenuation of seismic waves in two phase rocks, part 1: Theoretical formulation: *Geophysics*, **39**, p. 587-606.
- Mallarino, G., Beaubouef, R. T., Droxler, A. W., Abreu, V., and Labeyrie, L., 2006, Sea level influence on the nature and timing of a minibasin sedimentary fill (northwestern slope of the Gulf of Mexico): *AAPG Bulletin*, **90**, p. 1089-1119.
- Marion, D., Nur, A., Yin, H., and Han, D., 1992, Compressional velocity and porosity in sand-clay mixtures: *Geophysics*, **57**, p. 554-563.
- Mavko, G., 1980, Velocity and attenuation in partially molten rocks: *J.Geophys.Res.*, **85**, p.5173-5189.
- Mavko G., Mukerji T. and Dvorkin J., 1998, *The rock physics handbook: tools for seismic analysis in porous media*, Cambridge University press, 329.
- Mavko, G., and Mukerji, T., 1998: Comparison of the Krief and critical porosity models for prediction of porosity and V_p/V_s , *Geophysics*, **63**, p. 925-927.
- Miner, J. W., 1982, Clay models and acoustic velocities: SPE 11031, 57th Annual Fall Technical Conference and Exhibition of the SPE.
- Mindlin, R. D., 1949, Compliance of elastic bodies in contact: *J.Appl.Mech.*, **16**, p. 259-268.
- Murphy, W., Reischer, A., and Hsu., K., 1993, Modulus decomposition of compressional and shear velocities in sand bodies: *Geophysics*, **58**, p. 227-239.
- Nur, A., Mavko, G., Dvorkin, J., and Galmudi, D., 1998, Critical porosity: A key to relating physical properties to porosity in rocks: *The Leading Edge*, **17**, p. 357-362.
- O'Connell, R. J., and Budiansky, B., 1974, Seismic velocities in dry and saturated cracked solids: *J. Geophys.Res.*, **79**, p. 5412-5426.

- Odegaard, E., and Avseth, P., 2004, Well log and seismic data analysis using rock physics templates: *First Break*, **22**, p. 37-43.
- Schoenberg, M., 1983, Reflection of elastic waves from periodically stratified media with interfacial slip: *Geophys. Prospecting*, **31**, p. 265-292.
- Sheriff R., 2006, *Encyclopedic dictionary of applied geophysics*, fourth edition: Society of Exploration Geophysicists Tulsa, Oklahoma, USA.
- Smith, T., and Sondergeld, C. H., 2001, Examination of AVO responses in the eastern deepwater Gulf of Mexico: *Geophysics*, **66**, No. 6, p. 1864–1876.
- Smith, T. M., Sondergeld, C. H., and Rai, C. S., 2003, Gassmann fluid substitutions: A Tutorial: *Geophysics*, **68**, p. 430-440.
- Sullivan, M. D., Foreman, J. L., Jennette, D. C., Stern, D., Jensen, G. N., and Goulding, F. J., 2004, An integrated approach to characterization and modeling of deep-water reservoirs, Diana field, western Gulf of Mexico, in *Integration of outcrop and modern analogs in reservoir modeling: AAPG Memoir*, **80**, p. 215– 234.
- Thomas, E. C., Steiber, S. J., 1975, The distribution of shale in sandstone and its effect upon porosity, SPWLA, 16th Annual Logging Symposium, p. 1-17.
- Truman, R.B., Howard, W.E., and Luffel, D.L., 1989, Shale porosity - its impact on well log modeling and interpretation: SPWLA Symposium, 30th, Transactions, p. Q1-Q15.
- Vernik, L., 1998, Acoustic velocity and porosity systematics in siliciclastics: *The Log Analyst*, **39**, p. 27-35.
- Walton, K., 1987, The effective elastic moduli of a random packing of spheres: *J.Mech.Phys.Solids*, **35**, p. 213-226.
- Wang, Z., 2001, Fundamentals of seismic rock physics: *Geophysics*, **66**, p. 398–412.
- Wang, Z., Wang, H., and Cates, M. E., 2001, Effective elastic properties of clays: *Geophysics*, **66**, p. 428–440.
- Williams, D. M., 1990, The acoustic log as hydrocarbon indicator: *Ann. Logging Symp.*, SPWLA, paper W.
- Zimmer, M., Prasad, M., and Mavko, G., 2002, Pressure and porosity influences on V_p - V_s ratio in unconsolidated sands: *The Leading Edge*, **21**, p. 178-183.

APPENDIX I: Coordination number

Two aspects of granular media models can be discussed: one related to the type of physical assumptions of the contact surface between two identical spherical grains, and the other related to the coordination number (n). Murphy (1982) proposed an empirical n -porosity (Φ) relation based on various laboratory measurements (Figure 47). Murphy's n -porosity relation can be represented as follows (Mavko *et al.*, 1998):

$$n = 24.041 e^{-2.676 \Phi} \quad (27)$$

It is often used with the Hertz-Mindlin model to compute effective elastic moduli. The n in Murphy's relation is probably higher than the actual value due to the uncertainty in distinguishing between actual grain contacts and near-grain contacts.

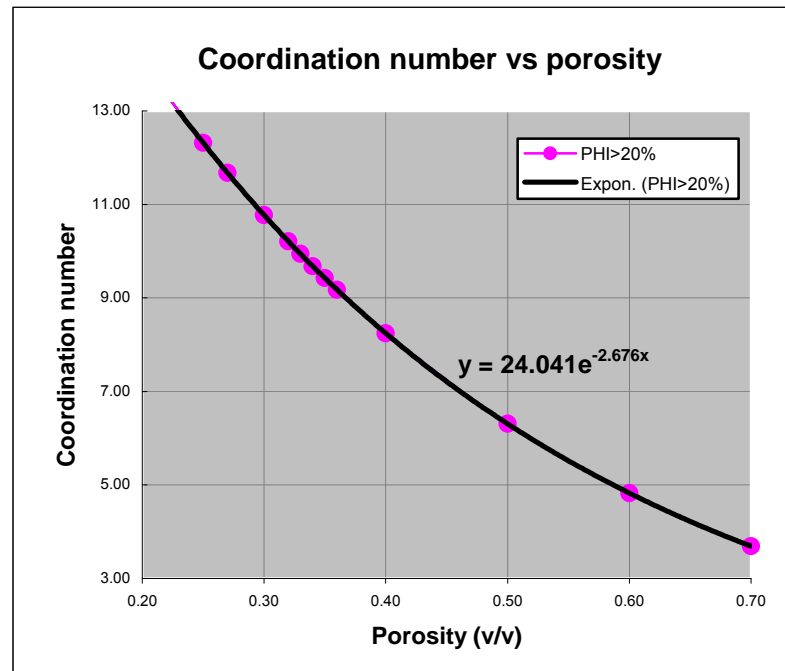


Figure 47. Geometric properties of sphere pack: coordination number vs. porosity.

APPENDIX II: Effective pressure estimation

Effective pressure was computed as the difference between overburden and pore pressure, using the following equation:

$$P_{eff} = P_{ovb} - \beta P_p \quad (28)$$

where,

P_{eff} = effective pressure;

P_{ovb} = overburden/confining pressure (with the gradient of 1 psia/ft);

β = Biot coefficient (assumed to be unity);

P_p = Pore pressure (~6770 psia, obtained from MDT data report, Figure 48).

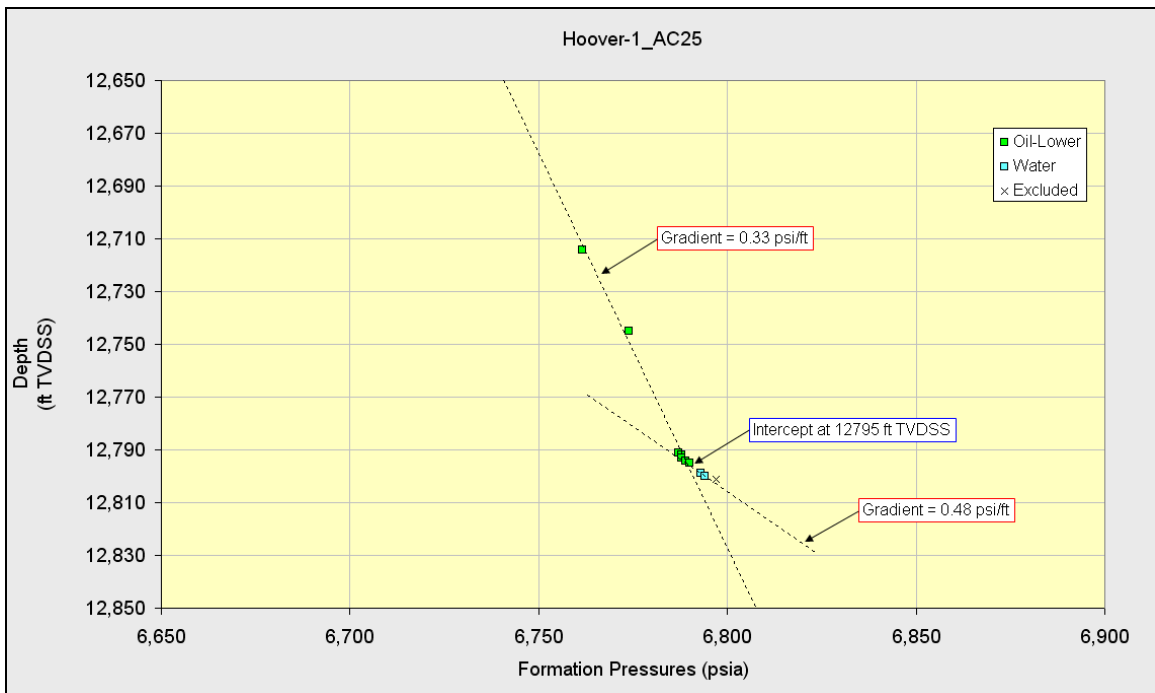


Figure 48. Pressure gradient analysis for Hoover-1 (MDT data).

APPENDIX III: Indonesia equation

As a part of petrophysical analysis, water saturation (S_w) was estimated using Indonesia equation given through following form:

$$\frac{1}{\sqrt{R_t}} = \left(\frac{V_{sh}^{1-0.5V_{sh}}}{\sqrt{R_{sh}}} + \frac{\Phi^{m/2}}{\sqrt{aR_w}} \right) * S_w^{n/2} \quad (29)$$

where,

R_t = true resistivity (usually deep resistivity reading);

V_{sh} = volume of shale;

R_{sh} = resistivity of shale;

Φ = porosity;

a = Archie's parameter: cementation factor;

m = Archie's parameter: cementation exponent;

n = Archie's parameter: saturation exponent;

S_w = water saturation.